

NAVAL POSTGRADUATE SCHOOL MONTEREY, CALIFORNIA



THESIS

VALIDATION OF
SPECIAL SENSOR MICROWAVE/IMAGER
OCEAN SURFACE WIND RETRIEVALS
IN EQUATORIAL REGIONS

by

Elton G. Sayward

December, 1994

Thesis Advisor:
Co-Advisor:

R. C. Olsen
M. C. Colton

Approved for public release; distribution is unlimited.

REPORT DOCUMENTATION PAGE

Form Approved OMB No. 0704-0188

Public reporting burden for this collection of information is estimated to average 1 hour per response, including the time for reviewing instruction, searching existing data sources, gathering and maintaining the data needed, and completing and reviewing the collection of information. Send comments regarding this burden estimate or any other aspect of this collection of information, including suggestions for reducing this burden, to Washington Headquarters Services, Directorate for Information Operations and Reports, 1215 Jefferson Davis Highway, Suite 1204, Arlington, VA 22202-4302, and to the Office of Management and Budget, Paperwork Reduction Project (0704-0188) Washington DC 20503.

1. AGENCY USE ONLY (Leave blank)		2. REPORT DATE Dec 1994.	3. REPORT TYPE AND DATES COVERED Master's Thesis	
4. TITLE AND SUBTITLE VALIDATION OF SPECIAL SENSOR MICROWAVE/IMAGER OCEAN SURFACE WIND RETRIEVALS IN EQUATORIAL REGIONS			5. FUNDING NUMBERS	
6. AUTHOR(S) Elton G. Sayward				
7. PERFORMING ORGANIZATION NAME(S) AND ADDRESS(ES) Naval Postgraduate School Monterey CA 93943-5000			8. PERFORMING ORGANIZATION REPORT NUMBER	
9. SPONSORING/MONITORING AGENCY NAME(S) AND ADDRESS(ES)			10. SPONSORING/MONITORING AGENCY REPORT NUMBER	
11. SUPPLEMENTARY NOTES The views expressed in this thesis are those of the author and do not reflect the official policy or position of the Department of Defense or the U.S. Government.				
12a. DISTRIBUTION/AVAILABILITY STATEMENT Approved for public release; distribution is unlimited.			12b. DISTRIBUTION CODE	
13. ABSTRACT (maximum 200 words) The Fleet Numerical Meteorology and Oceanography Center (FNMOC) has the charter to provide Special Sensor Microwave/Imager(SSM/I) data to DOD and NOAA users. This tasking has led to new methods for processing SSM/I data being developed to improve NAVY SSM/I products, in particular the ability to remotely sense ocean surface winds. Currently, alternative SSM/I ocean surface wind speed algorithms include 'physical' or 'statistical' methods. Typically "physical" retrievals require additional data, e.g., cloud liquid water, along with SSM/I brightness temperatures while statistical methods are standalone algorithms based on brightness temperature only. In this study four candidate wind retrieval methods proposed at the SSM/I Algorithm Symposium(June 1993) for implementation at FNMOC are examined. Limitations of the SSM/I calibration/validation data set to the mid-latitude region prompted the requirement to develop a tropical data set for evaluation of alternative algorithms. Comparison of SSM/I wind retrieval methods reveal neural networks display a high wind speed bias for winds above 11 m/s and a low wind speed bias for winds below 3 m/s. The current FNMOC operational algorithm may overestimates wind speeds when water vapor is greater than 50 kg/m ² . Partitioning of SSM/I retrieved wind speeds according to accuracy is by accomplished when using brightness temperature received at 37 GHZ.				
14. SUBJECT TERMS SSM/I Remote Sensing of Ocean Surface Winds			15. NUMBER OF PAGES 78	
16. PRICE CODE				
17. SECURITY CLASSIFICATION OF REPORT Unclassified	18. SECURITY CLASSIFICATION OF THIS PAGE Unclassified	19. SECURITY CLASSIFICATION OF ABSTRACT Unclassified	20. LIMITATION OF ABSTRACT UL	

Approved for public release; distribution is unlimited.

VALIDATION OF SPECIAL SENSOR MICROWAVE/IMAGER
OCEAN SURFACE WIND RETRIEVALS
IN EQUATORIAL REGIONS

by

Elton G. Sayward
Lieutenant, United States Navy
B.S., Southern Illinois University, 1983

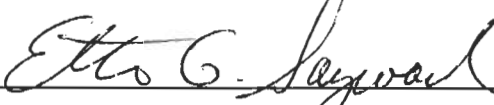
Submitted in partial fulfillment
of the requirements for the degree of

MASTER OF SCIENCE IN APPLIED PHYSICS

from the

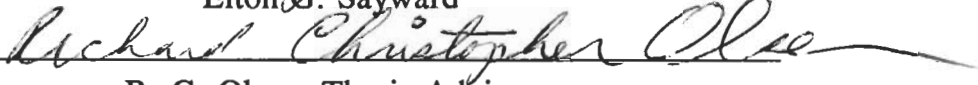
**NAVAL POSTGRADUATE SCHOOL
December 1994**

Author:




Elton G. Sayward

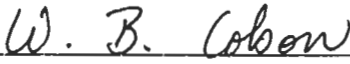
Approved by:



R. C. Olsen, Thesis Advisor



M. C. Colton, Co-Advisor



W. B. Colson, Chairman
Department of Physics

ABSTRACT

The Fleet Numerical Meteorology and Oceanography Center (FNMOC) has the charter to provide Special Sensor Microwave/Imager(SSM/I) data to DOD and NOAA users. This tasking has led to new methods for processing SSM/I data being developed to improve NAVY SSM/I products, in particular the ability to remotely sense ocean surface winds. Currently, alternative SSM/I ocean surface wind speed algorithms include 'physical' or 'statistical' methods. Typically "physical" retrievals require additional data, e.g., cloud liquid water, along with SSM/I brightness temperatures while statistical methods are standalone algorithms based on brightness temperature only.

In this study four candidate wind retrieval methods proposed at the SSM/I Algorithm Symposium(June 1993) for implementation at FNMOC are examined. Limitations of the SSM/I calibration/validation data set to the mid-latitude region prompted the requirement to develop a tropical data set for evaluation of alternative algorithms. Comparison of SSM/I wind retrieval methods reveal neural networks display a high wind speed bias for winds above 11 m/s and a low wind speed bias for winds below 3 m/s. The current FNMOC operational algorithm may overestimate wind speeds when water vapor is greater than 50 kg/m². Partitioning of SSM/I retrieved wind speeds according to accuracy is best accomplished by using brightness temperature received at 37 GHZ.

TABLE OF CONTENTS

I.	INTRODUCTION	1
II.	BACKGROUND	5
	A. THEORY	5
	1. Sources of Thermal Radiation	5
	2. Ocean Surface Microwave Emission	7
	3. Atmospheric Transmission	9
	B. SSM/I INSTRUMENT DESCRIPTION	11
	C. WIND RETRIEVAL METHODS	13
III.	STUDY PROCEDURES	19
	A. BUOY DATA SET	19
	B. SSM/I AND BUOY MATCHUP CRITERIA	20
IV.	OBSERVATIONS	23
	A. SSM/I WIND SPEED VS BUOY WIND SPEED	23
	B. PERFORMANCE RESULTS	25
	C. PARTITIONING OF RETRIEVED WIND SPEEDS	25
	D. WATER VAPOR EFFECTS	26
V.	ANALYSIS	27
	A. CV ALGORITHM	27
	B. NEURAL NETWORK WIND BIAS	27
	C. SENSITIVITY OF WIND SPEED RETRIEVAL METHODS	28
	D. PARTITIONING OF SSM/I GENERATED WIND SPEEDS	29
	E. CV ALGORITHM DEPENDENCE ON WATER VAPOR	29
VI.	CONCLUSIONS AND RECOMMENDATIONS	31
	APPENDIX A: FIGURES	33
	APPENDIX B: TABLES	63

LIST OF REFERENCES	67
INITIAL DISTRIBUTION LIST	69

ACKNOWLEDGEMENTS

The author would like to thank Professor R.C. Olsen for providing insight, advice and timely guidance. I wish to express my gratitude and appreciation to Dr. Marie Colton for enthusiasm, encouragement, and assistance throughout this study.

I would like to thank Gene Poe for providing the SSM/I data and Linda Magnum for making available the TOGA Buoy data. In addition I would like to thank Mark Goodberlet for allowing me to draw upon his past experience during the early stages of this work.

Most of all, to my wife Robin, thank-you for your unwavering support and faith during my two years in Monterey, CA.

I. INTRODUCTION

The ability to generate synoptic maps of wind speeds over the ocean on a global scale has been greatly enhanced through developments in the science of microwave radiometry. Microwave emissions are useful in remote sensing because of their capability to penetrate clouds and moderate rainfall. Aircraft and satellite observations demonstrate that microwave energy from the ocean surface can be remotely sensed by passive microwave radiometers (Swift,1977), and these emissions in turn used to develop algorithms to retrieve ocean surface wind speeds.

Early use of microwave radiometric techniques to evaluate the dynamics of the ocean surface from space was provided to researchers by the electrically scanning microwave radiometer systems aboard NIMBUS-5 (1972) and NIMBUS-6 (1975) satellites. In 1978 the first scanning multichannel microwave radiometers or SSMR were carried aboard the SEASAT-A and NIMBUS-7 satellites. The SMMR was able to provide observations of the sea-surface, sea-ice, and land parameters (Gloersen et al., 1984), except during moderate to heavy rainfall. The SSMR clearly demonstrated the capability to remotely sense near-surface ocean wind speeds (Wentz et al,1986).

Following the SMMR a Special Sensor Microwave/Imager (SSM/I), was built by Hughes Aircraft Company (HAC) under the direction of the Naval Space Systems Activity(NSSA) and the Air Force Space Division. The SSM/I represents a joint Navy/Air Force operational program to obtain synoptic maps of critical atmospheric, oceanographic, and selected land parameters on a global scale (Hollinger et al.,1987). The first SSM/I was launched in June of 1987 aboard the Defense Meteorological Satellite Program(DMSP) spacecraft F8. Improvements in the SSM/I over the SMMR include twice the swath width and higher frequency range for microwave energy detection.

Early wind speed retrieval for the SSM/I was accomplished utilizing a multichannel linear regression algorithm developed by HAC. This pre-launch algorithm required SSM/I channel outputs and the use of nine distinct climate codes representing a particular season and latitude band (Lo, 1983 and Hollinger et al., 1987). During the calibration and validation of the SSM/I, wind retrievals were correlated with buoy wind measurements with the results that the Hughes algorithm had a high wind speed bias, along with discontinuity problems across the latitude bands (Hollinger, et al., 1991). An alternate global wind speed algorithm was developed by Goodberlet et al.(1989) during the calibration/validation of the SSM/I, which is valid in all latitudes and during all seasons and meets DOD operations requirement of ± 2 m/s accuracy requirement under rain free conditions. The Goodberlet algorithm is the current operational algorithm at the Fleet Numerical Meteorological and Oceanography Center (FNMOC). Improvements in wind speed retrieval in the medium to high wind range (6-20 m/s) was accomplished by Goodberlet and Swift(1992) with modifications to the calibration/validation global algorithm. This improved algorithm, however produces inaccuracies at low wind speeds.

The use of neural networks(NN) to perform retrieval of parameters and classification of remote sensing data using SSM/I outputs was illustrated by Dawson and Fung(1993). The first NN developed for use with the SSM/I channel outputs was by Stogryn et al.(1994) and showed a 30% increase in wind speed retrieval accuracy in nonprecipitating conditions. More recently, a single "all-weather" NN was tested using the same data set as the Stogryn et al. NN and produced similar accuracies (Krasnopolsky, et al, 1994).

The regression algorithms and NN's used for generating ocean wind speed retrieval have all been developed and tested using the same SSM/I/buoy pair data base reflecting the first

year of F-8 operation(1987). This data set is limited to mostly mid-latitude regions and does not contain enough low wind and high moisture samples to completely validate wind retrieval methods. These limitations were brought out during the SSM/I Algorithm Symposium, held in June 1993, along with identifying the need for an expanded data set including moist, tropical regions and low winds to provide further validation of existing methods and determine which approach yields the most accurate wind retrievals over a wide range of environmental conditions.

The purposes of this study are:

- a) compile an expanded data set of SSM/I/buoy matchups in the equatorial regions
- b) evaluate performance accuracies of the following wind retrieval methods
 - Calibration Validation algorithm (CV)
 - Goodberlet and Swift improved algorithm (GS)
 - Stogryn, Butler, Bartolac NN (SBB)
 - Krasnoposky, Breaker, Gemmill NN (NMC)
- c) evaluate methods of partitioning retrieved wind speeds
- d) investigate CV algorithm positive wind speed bias dependence on high levels of water vapor in the atmosphere

The following chapter will present a discussion of the effect of ocean surface roughness on microwave emissions, a brief description of the SSM/I instrument and outline the evolution of the wind speed retrieval methods using SSM/I data. Chapter III will detail the methods used to generate wind retrievals and comparisons for this study. Chapter IV will discuss the results of wind speed retrievals comparisons with in-situ buoy values. Chapter V will analyze these results. Chapter VI will present conclusions and recommendations. All figures and tables are contained in Appendix A and B respectively.

II. BACKGROUND

A. THEORY

1. Sources of Thermal Radiation

Passive microwave remote sensing of the ocean surface is based on the premise that radiometric emission from the ocean surface varies with the amount of surface roughness, which is influenced by wind speed over the ocean. A technique for correlating wind speed over the ocean surface to microwave emission was developed through early analytical work, (Stogryn, 1972), later through experimental tests (Hollinger, 1971) and finally with aircraft and satellite data (Swift, 1977). This section will discuss some of the underlying physics involved with measuring ocean surface wind speeds.

For microwave frequencies the brightness or radiance of a blackbody at temperature 'T' is defined (Ulaby, et al.);

$$(1) \quad B(\nu, T) = \frac{2k\nu^2}{c^2} T \quad .$$

B = radiance
k = Boltzman Constant
 ν = frequency
T = temperature
c = speed of light

Equation 1 shows for a blackbody at thermal equilibrium the thermally emitted radiance is proportional to its temperature for a fixed frequency. In the case of the ocean, which is not an ideal blackbody, its thermal emission is reduced by its emissivity ' ϵ_s ' which is a function of incidence angle, sea surface temperature, and salinity.

The ocean radiance 'L' is;

$$(2) \quad L(\nu, T) = \frac{2k\nu^2}{c^2} [\epsilon_s T]$$

L = ocean radiance
 k = Boltzman Constant
 ν = frequency
 c = speed of light
 ϵ_s = ocean surface emissivity
 T = temperature

where the quantity in the brackets is defined as the Brightness Temperature ' T_B ', which is used in microwave radiometry to represent radiance. At frequencies greater than 5 GHz salinity does not contribute significantly to brightness temperature.

The thermal radiation spectrum received by a passive microwave radiometer (Figure 1) is comprised of four main components; 1) surface emissions, 2) upwelling atmospheric radiation, 3) reflected downwelling atmospheric radiation attenuated by atmospheric absorption, 4) reflected space radiation modified by the two way atmospheric absorption. The equivalent blackbody temperature of this radiation may be expressed (Swift, 1990);

$$(3) \quad T_B = \epsilon T e^{-\tau} + T_{up} + R T_{dn} e^{-\tau} + R T_{sp} e^{-2\tau}$$

where: T_B = total brightness temperature
 ϵ = emissivity of the ocean surface
 $e^{-\tau}$ = atmospheric attenuation
 R = reflectivity of ocean surface
 $T_{up} \approx T_{dn}$ = total atmospheric radiation
 T_{sp} = space radiation
 T = surface temperature

The quantity (τ) is the atmospheric opacity or the relative capacity of atmospheric constituents (oxygen, water vapor, clouds or rain) to obstruct the transmission of radiant

energy. At microwave frequencies (4-100GHZ) and under most atmospheric condition except moderate to heavy rain the opacity is small and the first term in Equation 3 (ocean surface emission) dominates.

2. Ocean Surface Microwave Emission

To determine the amount of microwave emission from the ocean surface, relationships maybe developed based on the assumption that the depth of ocean affected by microwave absorption and radiation is semi-infinite, homogeneous, and isothermal. The phenomenon that microwaves only penetrate to a skin depth of less than 1cm allow these approximations to be made. Since all transmitted energy is eventually absorbed in a semi-infinite, homogeneous conducting medium, absorption can be defined as:

$$(4) \quad A = 1 - R$$

A = absorption of microwave energy
R = reflectivity of ocean surface

If one further assumes the ocean surface is at thermal equilibrium, then the rate of emission(emissivity) from the surface is equal to the rate of absorption at the surface and Equation (4) can be written:

$$(5) \quad R = 1 - \epsilon$$

Where ' ϵ ' is the emissivity from the ocean surface.

For a calm sea surface microwave emissions as a function of incidence angle are highly polarized. Figure 2, shows for radiometric emissivity for vertical polarization is much larger than horizontal polarization at the SSM/I viewing angle of 53°. This large polarization difference is used to distinguish ocean surfaces from other surfaces(vegetation,snow) or atmospheric particles where scattering of the microwaves reduce polarization differences.

The reflectivity is broken down into the vertical and horizontal polarization coefficients using the Fresnel formulas:

$$(6a) \quad R_V = \left[\left| \frac{\epsilon_S \cos\theta - \sqrt{\epsilon_S - \sin^2\theta}}{\epsilon_S \cos\theta + \sqrt{\epsilon_S - \sin^2\theta}} \right| \right]^2$$

$$(6b) \quad R_H = \left[\left| \frac{\cos\theta - \sqrt{\epsilon_S - \sin^2\theta}}{\cos\theta + \sqrt{\epsilon_S - \sin^2\theta}} \right| \right]^2$$

R_V = vertical polarization
 R_H = horizontal polarization
 ϵ_S = relative dielectric constant

The effects of a rough ocean surface have not been accurately modeled, due to the difficulty of characterizing the shape of the wind-roughened surface and the complexity of electromagnetic interactions with any reasonably realistic representation of the shape. Consequently, empirical corrections are based on experimentally derived relationships between brightness temperatures and wind speed.

There are three mechanisms that affect emissivity from a rough ocean surface. The first of these is from surface waves having long wavelengths compared to the radiation wavelength. These surface waves change the local incident angle (Wentz, 1992) and mix the horizontal and vertical polarization states. A second roughness mechanism is the diffraction of microwaves by surface waves that are small compared to radiation wavelength, called Bragg diffraction. The third mechanism is foam from breaking waves, a mixture of air and water.

surface. At low incidence angles ($< 20^\circ$), specular reflections from long ocean waves of comparable slope dominate. In the incidence angle range of 20° to 60° Bragg roughness effects dominate ocean surface emissions. As foam forms on the ocean higher brightness temperatures are generated by the behavior of foam, which is similar to that of a blackbody with emissivity near one.

Horizontally polarized brightness temperatures for rough and foam covered ocean surface show an increase over smooth surface values, regardless of radiometer viewing angle (Hollinger, 1971). Vertical polarized brightness temperatures do not vary monotonically with angle; for rough ocean surfaces at viewing angles less than 50° vertical polarization temperature increases with roughness. At viewing angles greater than 50° vertical polarization values decrease for rough ocean surface. It is because of this phenomenon that space radiometers view the ocean surface at approximately 50° to minimize surface roughness effects and increase sensitivity in brightness temperature to foam generation. It was shown through the compilation of four oceanographic studies (Figure 3), that percentage of foam does increase with increasing wind speed, (Stogryn, 1972) and hence there is a relationship for deriving wind speed over the ocean and brightness temperature received by a passive radiometer.

3. Atmospheric Transmission

Most microwave remote sensing systems operate in the 3 to 30 GHz range (super-high-frequency). This region offers the least attenuation effect by the atmosphere (Figure 4). It would appear from Figure 4 the lower frequencies ($< 10\text{GHz}$) would be best for surface observations. There are several reasons why this is not the case. At approximately 22GHz there is a water vapor absorption line that is used exclusively for radiometric sensing as an indicator of the amount of water vapor in the atmosphere. An increase in water vapor can result

in an increase of up to 100°K in brightness temperature at 22GHz on very humid days(Swift,1990). Some geophysical observations require higher frequencies. For example, to discriminate new sea ice from old sea ice a choice of both a low frequency(< 18GHz) and high frequency at 35GHz is required. Another reason for selecting higher frequencies is the need to improve spatial resolution from orbital altitudes. The spatial resolution of a microwave radiometer may be defined as;

$$(7) \quad \Delta = \frac{\lambda H}{D} .$$

Δ = spatial resolution
 H = orbital altitude
 D = diameter of antenna
 λ = operating wavelength

The orbital altitude is fixed and there is a limit to the size of antenna of a spacecraft. Spatial resolution is then dependent on wavelength. A ten-fold improvement in spatial resolution can be achieved by using 35GHz as opposed to 3.5 Ghz. The tradeoff comes as a decrease in accuracy of surface observations due to an increase in atmospheric attenuation at higher frequencies. An increase in brightness temperature may be the result of a change in ocean surface roughness, water vapor or cloud cover. Since frequency response of clouds and water vapor are known functions of wavelength, the use of three wavelengths, for example at 19GHz, 22Ghz, and 35Ghz can be used to correct for atmosphere effects.

This section discussed the strong correlation between wind speed and surface emissivity in the microwave spectrum. Also, it was shown how brightness temperature detected by a passive radiometer depends on frequency, polarization and viewing angle.

B. SSM/I INSTRUMENT DESCRIPTION

The first SSM/I instrument was flown aboard the DMSP F8 satellite in 1987 (Figure 5). In Figure 5 the SSM/I is shown in the deployed position. Today, SSM/I instruments are aboard three other DMSP satellites designated F10, F11 and F12. This study used SSM/I data from the F8 and F10 spacecrafts.

The DMSP satellites are in a sun-synchronous near-polar orbit at an altitude of approximately 833 km (Figure 6). The spacecraft has an orbital angle of inclination relative to the equatorial plane of 98.8° and an orbit period of 102 minutes, producing 14.1 full orbit revolutions per day. The radiometer scans conically at an angle of 45 degrees from the spacecraft resulting in an observation angle of incidence of approximately 53.1° . The SSM/I rotates continuously at 31.6 rpm about an axis parallel to the local vertical and measures surface brightness temperature over an angular sector of 102.4° about the sub satellite track. The scan direction is from left to right when looking in the aft direction of the spacecraft with an active scene measurement lying $\pm 51.2^\circ$ about the aft direction. This results in a swath width of 1400 km. The SSM/I moves along the sub satellite track in the negative 'Y' direction at 6.58 km/sec which results in a separation between successive scans of 12.5 km along the satellite track direction and is nearly equal to the resolution of the 85 GHz beams. During each scan 128 uniformly spaced samples of the 85.5 GHz channels are taken over the scan region. Radiometer data at the remaining frequencies are sampled every other scan with 64 uniformly spaced samples being taken. Scan A denotes scans in which all channels are sampled while B denotes scans in which only the 85.5 GHz data is taken.

Figure 7 shows the satellite subtrack coverage over successive days. There are small unmeasured circular sectors of 2.4 degrees at the north and south poles, (Hollinger 1991). One spacecraft will not cover the entire surface every day, but horizontal coverage is dense enough for deriving wind speeds over most of the oceanic areas up to two times per day, (Schluessel et al., 1991).

The SSM/I is a seven-channel, four frequency, linearly polarized passive microwave radiometer. The instrument receives vertically polarized radiation at 22.2GHZ and both vertically and horizontally polarized radiation at 19.3, 37.0 and 85.5GHZ. The 19.3, 22.2, 37.0 and 85.5GHZ frequencies are used for reasons previously discussed and as summarized in Table 3 in Appendix B.

Seven separate channels are employed by the SSM/I to simultaneously measure microwave emission from the Earth and through the atmosphere. The antenna system consists of an offset parabolic reflector focusing the earth's radiation into a broadband, seven port feedhorn. This assembly, including parabolic reflector, feedhorn and receiver, spins about an axis parallel to the local spacecraft vertical at a period of 1.9s. Attached to the spin axis but not rotating are a cold sky reflector and warm reference load. With this arrangement the feedhorn assembly will sense the fixed cold reflector and warm load once each scan. This allows in flight calibration observations to be taken every scan and represents a significant improvement over previous passive microwave radiometers. A more detailed description of the SSM/I hardware is provided in Hollinger et al. (1987).

C. WIND RETRIEVAL METHODS

The original linear wind speed algorithm(DMatrix), developed for use with the F8 SSM/I is shown below, (Lo, 1983):

$$(8) \quad SW = C_{0j} + C_{1j} \cdot T_B(19H) + C_{2j} \cdot T_B(22V) \\ + C_{3j} \cdot T_B(37V) + C_{4j} \cdot T_B(37H)$$

Equation (8) is valid only over open ocean and generates wind speed, SW, in meters/seconds(m/s) referenced to a height of 19.5m above the surface. The T_B 's represent brightness temperatures in degrees Kelvin at SSM/I retrieved frequencies and polarizations. The coefficients C_i represent values as a function of climate codes 'j' that are based on the season and latitude band of the received SSM/I data.

A concern with wind retrieval using microwave emission was the effect of rain attenuating the energy from the ocean surface and the resulting accuracy of the wind speed generated. With this in mind a "rain flag" was developed for the purpose of identifying varying degrees of attenuation due to rain in the atmosphere. The rain flag criteria for Equation 8 are :

$$\begin{aligned} \text{IF: } T_B(19H) > 190K \\ \text{OR: } [T_B(37V) - T_B(37H)] < 25K \\ \text{Then possible rain exists and rain flag} = 1 \\ \text{IF: } [T_B(37V) - T_B(37H)] < 10K \\ \text{Then heavy rain exists and rain flag} = 2 \\ \text{Otherwise rain flag} = 0 \end{aligned}$$

It is worth noting that the original algorithm did not attempt to calculate winds under rain flag condition 2, (Hollinger, 1991).

One of the requirements during the calibration/validation of the first SSM/I instrument was to verify the ability of the wind speed algorithm to meet wind speeds to accuracies of ± 2 m/s. This process was accomplished by comparing SSM/I wind retrievals to coincident surface wind speed measurements from ocean buoys(Figure 8).

The comparisons showed the wind speed algorithm did not meet the specified accuracy requirement of ± 2 m/s. Using linear regression on paired buoy wind speeds and SSM/I brightness temperatures, a set of new coefficients for the algorithm were developed (Hollinger, 1991). The accuracy specifications were met (Figure 9), but the revised climate coded algorithm still underestimated high wind speeds and produced discontinuities across climate code boundaries (Goodberlet et al., 1989).

These problems were partially solved using a global algorithm or CV algorithm, which utilized a single set of coefficients, valid in all latitudes and seasons:

$$(9) \quad SW = 147.9 + 1.0969 \cdot T_B(19V) - 0.4555 \cdot T_B(22V) \\ - 1.7600 \cdot T_B(37V) + .7860 \cdot T_B(37H)$$

This algorithm was developed (Goodberlet et al., 1989) using a weighted linear regression, where weights used in the regression were set equal to one over the square root of the wind speed density, evaluated at a particular buoy wind speed. This type of weighting has the effect of making all wind speed ranges equally important in the development of the CV algorithm. An unweighted regression tends to emphasize wind speed ranges with the greatest amount of data and make the algorithm less sensitive to ranges where there are less data. The CV algorithm uses $T_B(19V)$ not $T_B(19H)$ since it resulted in more accurate retrievals. Additionally a more restrictive set of rain flags were introduced;

Rain Flag	Criteria	Accuracy
0	$T_B(37V) - T_B(37H) > 50$ AND $T_B(19H) < 165$	< 2 m/s
1	$T_B(37V) - T_B(37H) < 50$ OR $T_B(19H) > 165$	2 - 5 m/s
2	$T_B(37V) - T_B(37H) < 37$	5 - 10 m/s
3	$T_B(37V) - T_B(37H) < 30$	> 10 m/s

These rain flags are shown in Figure 10 with the horizontal axis representing $\Delta 37$ or $T_B 37V - T_B 37H$ and the vertical axis representing $T_B 19H$. Use of the CV algorithm removed zonal discontinuities, while still meeting accuracy specifications and high wind speed bias was removed (Figure 11). This is the current operational algorithm at FLENUMMETOCEN. However, the CV algorithm overestimates wind retrievals as $(T_B(37V) - T_B(37H))$ decreases in value, i.e. in an increasingly water-laden atmosphere.

Improvements in wind speed retrievals under adverse environmental conditions (Figure 12) was partially achieved by Goodberlet and Swift (1992), in the medium to high wind speed range (6-20 m/s). The Goodberlet Swift algorithm or GS algorithm involves the use of a nonlinear relationship between $T_B 37V$ and $T_B 37H$ which in part accounts for a decrease in wind speed bias. The GS algorithm is shown below

$$(10) \quad W_{GSM} = \frac{W_G - 18.56 \cdot \alpha}{1.0 - \alpha}$$

$$(11a) \quad W_G = SW = 147.90 + 1.0969 \cdot T_B(19V) - .4555 \cdot T_B(22V) \\ - 1.7600 \cdot T_B(37V) + .7860 \cdot T_B(37H), \text{ and}$$

$$(11b) \quad \alpha = \left(\frac{30.7}{\Delta 37} \right)^4$$

$$\Delta 37 = T_B 37V - T_B 37H$$

From Equation (10) and as stated by Goodberlet and Swift the GS algorithm should not be used if the $T_B 37$ differential is less than 31K, but is highly reliable when $(T_B(37V) - T_B(37H))$ is greater 40K. The GS algorithm may overestimate low winds.

The first nonlinear algorithm neural network (NN) trained on a set of SSM/I brightness temperatures matched with buoy winds was developed by Stogryn, Butler, Bartolac (1994) and will be called the SBB NN throughout this study. Stogryn et al. partitioned the data set originally compiled by

Goodberlet et al. (1989) for the calibration/validation of the SSM/I instrument into two sets, one for network training and the other for network testing. SSM/I channels used to train the NN were 19.3(V)GHZ, 22.2(V)GHZ, 37.0(V)GHZ, and 37.0(H)GHZ.

The training/test sets were further divided into three subsets. The first contained all SSM/I buoy matchups where

$$T_B(37V) - T_B(37H) > 50K$$

and this subset was treated as 'clear' conditions.

The second subset included SSM/I buoy matchups that were termed 'cloudy';

$$T_B(37V) - T_B(37H) \leq 50K$$

$$T_B(19V) < T_B(37V)$$

$$T_B(19H) \leq 185K$$

$$T_B(37H) \leq 210K$$

The third subset is comprised of those matchups exceeding the above cloudy conditions and could be so overshadowed by atmospheric attenuation, generation of wind speeds using SSM/I data may not be possible.

Using two separate NNs and the partitioned data set, the SBB NN claimed a 30% improvement in wind retrieval accuracy for clear conditions over earlier linear and nonlinear algorithms and a 250% improvement in cloudy conditions. One of the drawbacks to this NN is the potential discontinuity between clear and cloudy regimes.

The most recently developed NN for possible use with SSM/I wind speed retrieval is that of the Krasnopolsky, Breaker, Gemmill (1994), which was trained over the entire range of buoy and SSM/I matchups rather than clear or cloudy subsets. This NN, called NMC (National Meteorological Center), when compared to buoy measurements produced a bias of less than 0.05m/s and a rms value of ≈ 1.65 m/s (Figure 13). Krasnopolsky et al. claimed even more accurate wind retrievals were possible if a moisture retrieval rain flag as a function

of cloud liquid water was used to partition data into good or bad sets, rather than using brightness temperatures values as done by the CV, GS algorithms and the SBB NN. One set would contain data used to generate wind speeds and the second containing data not to be used due to attenuation by atmospheric conditions.

III. STUDY PROCEDURES

SSM/I wind speed retrievals from the DMSP F8 and F10 spacecrafts were taken over a 3 month period from September 91 to December 91 and compared to in-situ buoy wind speed measurements. SSM/I wind retrievals were generated using the CV and GS algorithms and SBB and NMC neural networks.

A. BUOY DATA SET

For this work buoy data were obtained from the Pacific Marine Environmental Laboratory (PMEL) which collects data measured by the Tropical Ocean Global Atmosphere (TOGA) buoys. TOGA buoys are located in the Pacific equatorial region (Figure 14). Table 1 in Appendix B provides a listing of the TOGA buoy locations used for this study.

The parameters collected from the buoys included: wind speed, air temperature, sea surface temperature and relative humidity. TOGA moored-buoy wind measurements were made at a height of 3.8 meters above the ocean surface. A propeller-vane anemometer sampled wind speeds and recorded vector averaged east-west and north-south components. Pre- and postdeployment wind tunnel tests indicate accuracies of propeller-vane measurements to be within 0.2 m/s (Hayes et al., 1991).

All anemometer measurements were converted to an equivalent neutral wind speed defined to be the wind speed 19.5 meters above the surface. Smith's (1988) open ocean drag coefficient was used. This conversion was necessary to allow buoy wind speeds to be directly compared to SSM/I generated wind speeds which predict wind speeds at a height of 19.5 meters above the ocean surface. Wind speed varies non-linearly with height above the ocean (Figure 15). Figure 15 illustrates the conversion of a buoy measured wind speed of 5 m/s to neutral wind speeds as a function of height above the ocean surface.

The buoys were chosen to be further than 100 km from land to prevent land contamination of brightness temperatures that might occur from SSM/I antenna side lobes, and to ensure land did not restrict wind speed fetch distance for creating fully developed seas (Ulaby et al., 1986).

The wind speed distribution (Figure 16) of the TOGA buoys collected over this 3 month period agrees in form with the wind speed density distribution used in the calibration/validation data set used in the development of the aforementioned wind retrieval methods. TOGA buoy wind speeds ranged from a maximum of 12 m/s to a minimum value of 0 m/s with the majority of the winds occurring around 6 m/s.

B. SSM/I AND BUOY MATCHUP CRITERIA

Matched pairs of SSM/I wind retrievals and converted neutral buoy wind speeds were produced. This process was similar to that developed and implemented during the calibration/validation of the SSM/I instrument, (Hollinger, 1991). Data were selected for SSM/I data retrievals within 25 km of the buoy location, with a further restriction that the time of satellite acquisition was within 30 minutes of buoy wind speed measurement. The required accuracy of the SSM/I wind retrieval is ± 2 m/s when compared to buoy measured wind. The effect of the spatial and temporal match-up criteria increases the total standard deviation allowed by less than 10% as discussed by Monaldo(1988) and represents a small contribution to the overall error. SSM/I geolocation problems reported by Hollinger(1991), resulting in positioning errors of 6-7 km will not significantly effect wind speed comparisons due to the possible 25km spatial separation between SSM/I observation and buoy location.

There were normally several wind speed retrievals associated with each SSM/I overpass of a buoy location that would meet the matchup criteria. For this study, these

multiple SSM/I matchups were dealt with by using three different methods of generating a SSM/I wind speed retrieval to be used for buoy measured wind speed comparison. First, as had been done in the calibration/validation process a nearest neighbor approach was taken. Only one retrieval from each SSM/I overpass of a buoy location was used. Second, a straight average of all wind retrievals that met the matchup criteria from the SSM/I overpass was used to generate an average wind retrieval for comparison. Third, an inverse distance weighted average of the brightness temperatures were computed. The accuracy of these three methods are discussed in Chapter IV.

IV. OBSERVATIONS

A. SSM/I WIND SPEED VS BUOY WIND SPEED

A plot of SSM/I CV generated wind speeds vs buoy wind speeds is presented in Figure 17 and displays 12281 points meeting the temporal and spatial requirements with respect to coincident buoy position and wind speed measurement. No "rain flags" have been applied to the data. A least squares fit is calculated and displayed along with a diagonal line. In Figure 17 the majority of the CV values are approximately 1m/s too low, but at low wind speeds the CV algorithm overestimates wind speed values. In the ideal case, the data, or at least the fit, should be along the diagonal.

Figures 18 - 20 represent similar scatter plots for the GS algorithm and SBB, NMC NN's. The GS algorithm values in Figure 18 show the same characteristics as the CV data, but with a more pronounced underestimation of wind speeds ($\approx 1-2$ m/s) where the bulk of the data occurs. In comparison to the CV algorithm generated wind speeds in Figure 17, both NN's generate wind speeds lower than the in-situ buoy measurements where the buoy wind speed distribution is most dense (5-10m/s). A high wind speed bias underestimating all wind speeds above 11 m/s is displayed by SBB and NMC NN's in Figures 19 and 20. In Figure 20 a low wind bias overestimating winds below 3m/s is seen for the NMC NN. Overall the GS algorithm has the greatest underestimation of wind speed in comparison to the other retrieval methods.

The next series of Figures 21,22,23, display the error in SSM/I retrieved wind speeds vs buoy wind speed. For these plots the nearest neighbor values from each SSM/I and buoy coincident matchup set were used, which results in 584 observations. In Figure 21 CV "rain flags" 0, 1, 2, 3 are represented by dots, diamonds, squares and crosses respectively. In Figure 22 SBB "rain flags" clear, cloudy,

very cloudy are represented by dots, diamonds, and crosses respectively. Figure 23 does not have any associated rain flags since Krasnopolsky et al. developed the NMC NN without partitioning the data based on any atmospheric moisture conditions. In Figure 21, for rain flag 0, the CV algorithm generates an even distribution of wind speeds and does not display a bias until atmospheric conditions start to deteriorate as indicated by increasing rain flag values. With increasing rain flag the CV algorithm does overestimate wind speeds. The SBB NN(Figure 22) regardless of rain flag generated all SSM/I wind speeds lower than buoy measured winds when buoy wind speeds were greater than 11 m/s and generated all SSM/I wind speeds greater than buoy winds for buoy winds less than 2 m/s. The NMC NN(Figure 23) which does not use a rain flag produced similar bias as those seen with the SBB NN.

To get a better appreciation for variability among SSM/I retrieved wind speeds Figure 24 was developed to show the range of SSM/I values for 50 matchups of buoy and SSM/I data. In Figure 24 the horizontal axis represents nearest neighbor values and the vertical axis average values of SSM/I retrieved wind speeds. The vertical line associated with each matchup represents the range between the minimum and maximum values for that particular matchup. Note that the range in any single set of values is greater than the required ± 2 m/s accuracy.

A comparison of the four SSM/I wind retrieval methods(Figure 25), reveals as one might expect, the two NN's generate similar values, as do the CV and GS algorithms. In the first row, second column window, the vertical axis represents CV wind speeds with a range of 0 - 15 m/s and the horizontal axis SBB wind speeds with a range of 0 - 15 m/s. In this scatter plot NN generated wind speeds are equal to or less than CV generated wind speeds. This holds true for any comparison of either NN to CV or GS generated wind speeds.

B. PERFORMANCE RESULTS

Performance of the four wind speed retrieval methods under rain flag 0 conditions using nearest neighbor, average and weighted average retrieved wind speeds is displayed in Table 2. The data for Table 2 was obtained from scatter plots like Figure 26, where the legend in the lower right hand corner is interpreted as follows: # obs gives the number of data points in the plot, SD is the standard deviation of the quantity (SSM/I wind speeds - Buoy wind speeds), bias indicates the y-axis intercept, cor is the correlation coefficient between buoy winds and SSM/I generated winds and slope is that of the linear least squares fit of SSM/I wind speeds to the buoy wind speeds. The horizontal axis represents the range of buoy wind speed measurements and the vertical axis represents SSM/I wind speeds retrieved using CV or GS algorithms and SBB or NMC NN's. For each method a plot was generated for nearest neighbor(nn), average(ave), and weighted average(Wave) for comparison to buoy wind speeds.

Table 2 shows for individual methods using wind speeds values of nn, ave or Wave did not make a significant difference in bias and slope, but ave and Wave did yield better results for standard deviation and correlation values. Overall the NN's fare slightly better in standard deviation, bias and correlation values, but the NMC NN's slope is the lowest of any of the four retrieval methods.

C. PARTITIONING OF RETRIEVED WIND SPEEDS

A comparison of partitioning data as a function of T_B discriminates, water vapor(WV), cloud liquid water(CW), and relative humidity(RH) was conducted in an effort to determine if a physically based rain flag(WV,CW,RH) was a better partitioner of SSM/I retrieved wind speed accuracy than brightness temperatures. Relative humidity values were obtained from the TOGA buoy data, while WV and CW values are

computed from algorithms using brightness temperatures from channels 22.2 Ghz and 85.5GHz. Water vapor is the gaseous atmospheric water constituent and cloud liquid water is that portion of the liquid atmospheric water consisting of water droplets too small to precipitate, generally as having radii less than 100 microns.

In Figure 27, the plot on the left displays the difference between T_{B37V} and T_{B37H} vs buoy wind speed. Clear, cloudy and very cloudy rain flag conditions corresponding to the SBB NN "rain flags" are represented by dots, diamonds and crosses respectively. Separations among the three rain flag conditions occur at $\Delta 37 > 50$ and $\Delta 37 \approx 38$. The plot on the right of water vapor vs buoy wind speed shows a mixing of all three conditions. Plots of cloud liquid water vs buoy wind speed and relative humidity vs buoy wind speed yielded similar results as water vapor displaying a mixing of clear, cloudy and very cloudy conditions.

D. WATER VAPOR EFFECTS

To investigate the effects, if any, of increasing water vapor on accuracy of CV generated wind speeds a plot of CV accuracy vs water vapor was developed. In Figure 28 rain flag 0 conditions are represented by dots, rain flag 1 by diamonds, rain flag 2 by squares and rain flag 3 by crosses. It can be seen at water vapor greater than 50 kg/m^2 there is an increase in the overestimation of wind speeds and these data points are correctly flagged as 1,2,3. Additionally there are rain flag 0 data points in this region displaying a difference between buoy measured winds and CV generated wind of up to 8 m/s.

As discussed previously one of the criteria for rain flag 0 is $T_{B37V} - T_{B37H} > 50K$, Figure 29 is a plot of how this value changes with increasing water vapor. There is an area where the difference in T_{B37} 's are greater than 50K (rain flag 0) and water vapor values are greater than 50 kg/m^2 .

V. ANALYSIS

The purpose of this chapter is to explain why the four wind retrieval methods yielded their particular results. Areas examined included; impact of original calibration/validation data set limitations, weighting of TOGA data set wind speed distribution and use of rain flags in retrieval accuracy.

A. CV ALGORITHM

The CV algorithm displayed the least amount of wind speed bias over the largest range of winds compared to the other retrieval methods. This is attributed to the wind speed density weighting distribution used by Goodberlet et al. (1989) in the development of the CV algorithm. This algorithm does overestimate winds below 2.5 m/s regardless of rain flag, probably due to the limited number of low winds (< 3m/s) available in the original data set used to develop the coefficients for the CV algorithm.

B. NEURAL NETWORK WIND BIAS

Both NN's have a high and low wind speed bias. This underestimation of high winds (>11m/s) and overestimation of low winds (<3m/s) are attributed to two factors. First, the NN's are training set dependent. If the data set used to train a neural network is limited to a certain range of values, then the NN can only extract values in this range. In the case of the SBB and NMC NN's the limited calibration/validation data set apparently did not contain a large enough number of high wind speeds (>15m/s) and low wind speeds (<3m/s). Second, SBB and NMC NN's do not currently take into account the density of the buoy wind speed distribution of the training data set in their development.

That is, using the nomenclature of Stogryn et al., the neural networks minimize the following error function to determine the network coefficients for coincident SSM/I buoy matchups;

$$(12) \quad C = \sum_k a_k [S_{b,k} - S_k]^2$$

In Equation 12, $S_{b,k}$ is the buoy wind speed in meters per second for the k th match with SSM/I data, S_k is the corresponding estimate of the wind speed obtained by the network using matched brightness temperatures and a_k is wind speed density distribution weighting factor. Where CV and GS regression algorithms weight by the number of observations within a wind speed range, the neural networks use a uniform distribution, a_k equals 1. Stogryn et al. did experiment with weighting the wind speed distribution and claimed no change in accuracy of wind speeds retrieved, but was unable to explain this result.

C. SENSITIVITY OF WIND SPEED RETRIEVAL METHODS

Throughout this study the NN's have consistently generated low wind speeds when compared to in-situ buoy measured winds, with the exception of very low wind speeds. This, again reflects the limitation of the original training data set and the ability to incorporate the benefits of a weighted distribution. In Figure 25 it was seen how NN's generate low wind speeds when compared to either regression algorithm. The regression algorithms are more sensitive to high and low wind speeds. This is probably due to the non-uniformity weighting of the buoy wind speed distribution during CV algorithm development, (Goodberlet, 1992). The NN's are more accurate where the tropical wind speed density distribution is greatest and are significantly less sensitive at the extremes of the wind speed distribution.

D. PARTITIONING OF SSM/I GENERATED WIND SPEEDS

For this data set in the equatorial region the best discriminator for accuracy of wind speeds resulted from using the difference between the vertical and horizontal T_B37 values. With respect to WV and CW there was a mixing of clear, cloudy, and very cloudy/rainy conditions. WV and CW values are derived quantities using algorithms that include received brightness temperatures (19H, 22V, 37V, 37H), whereas the T_B37 values are basically in-situ measurements and have not had any algorithm filtering applied.

E. CV ALGORITHM DEPENDENCE ON WATER VAPOR

In some instances, wind speeds generated by the CV regression algorithm that were rain flagged 0 (predominantly clear conditions) failed to meet the $\pm 2\text{m/s}$ requirement, when wind speed retrieval was attempted under conditions of water vapor greater than 50 kg/m^2 .

VI. CONCLUSIONS AND RECOMMENDATIONS

Although all four SSM/I wind retrieval methods meet accuracy requirements of ± 2 m/s under rain flag 0 conditions; CV and GS algorithms are simpler in concept and easier to maintain than neural networks. Regression algorithms generate accurate wind speeds, especially if a stratification of rain flags reflecting accuracy is used. CV and GS algorithms are sensitive to a large range of wind speeds and are standalone algorithms, which do not require additional data, e.g., sea surface temperature along with brightness temperatures. To eliminate overestimation of low wind speeds a new set of coefficients need to be generated for the CV algorithm that can retrieve accurate wind speeds under rain flag 0 conditions for winds below 3 m/s. The current operational algorithm was found to exhibit in some instances an overestimation of retrieved winds at high water vapor levels (>50 kg/m²). re-evaluation of the CV rain flag 0 is required to remove these winds, but retain accurate retrievals. SBB and NMC NN's did not show a dependence on WV and in instances of high water vapor levels may be the preferred method of wind retrieval.

Both NN's reflected limitations of their training data set with generation of high and low wind speed bias. To solve this problem, it is necessary to compile a training set of SSM/I and buoy matchups including a large range of wind speeds. Until this is accomplished a non-uniform weighting distribution in Equation 11 may improve wind retrieval by NN's at high and low wind speeds. SBB and NMC NN's were most accurate where the wind speed density distribution is the greatest. From the data set used in this study, a combination of NN's and regression algorithms would provide more accurate wind retrievals over a larger range of wind speeds.

APPENDIX A: FIGURES

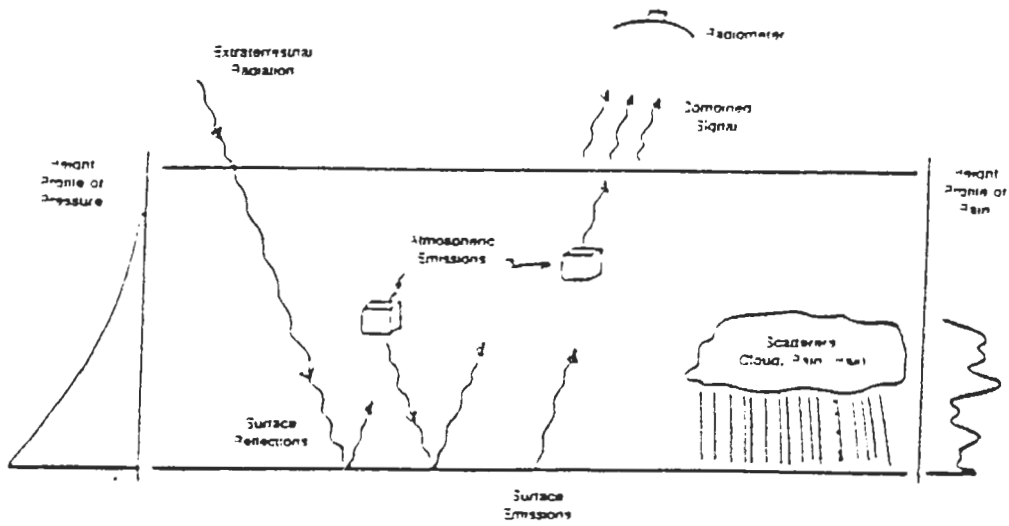


Figure 1: Sources of Thermal Radiation, From [Swift,1990]

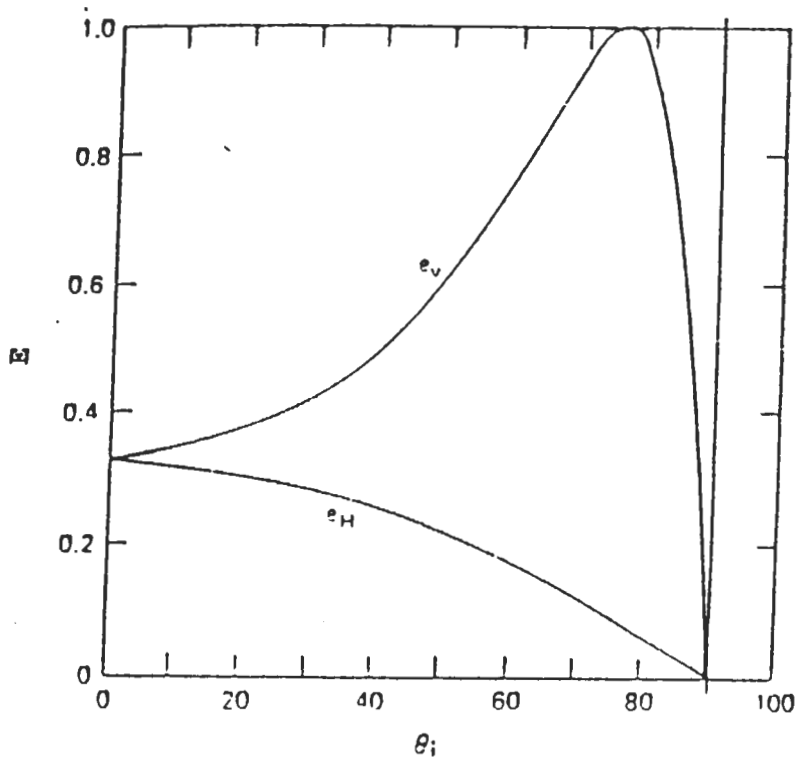


Figure 2: Incidence Angle Polarization Effects, From [Swift,1990]

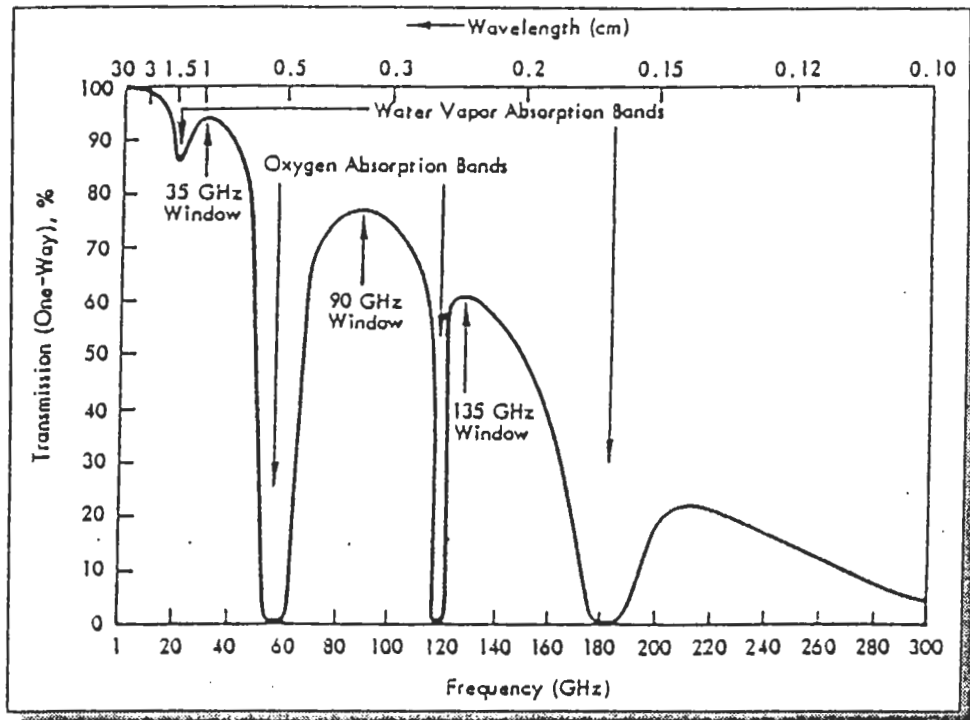


Figure 4: Atmospheric Attenuation, From [Ulaby, 1986]

SSM/I SENSOR

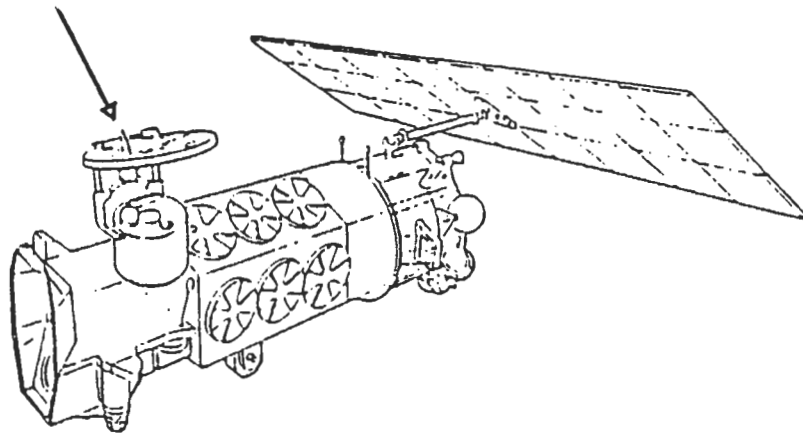


Figure 5: SSM/I on DMSP Satellite, From [Hollinger et al.,1987]

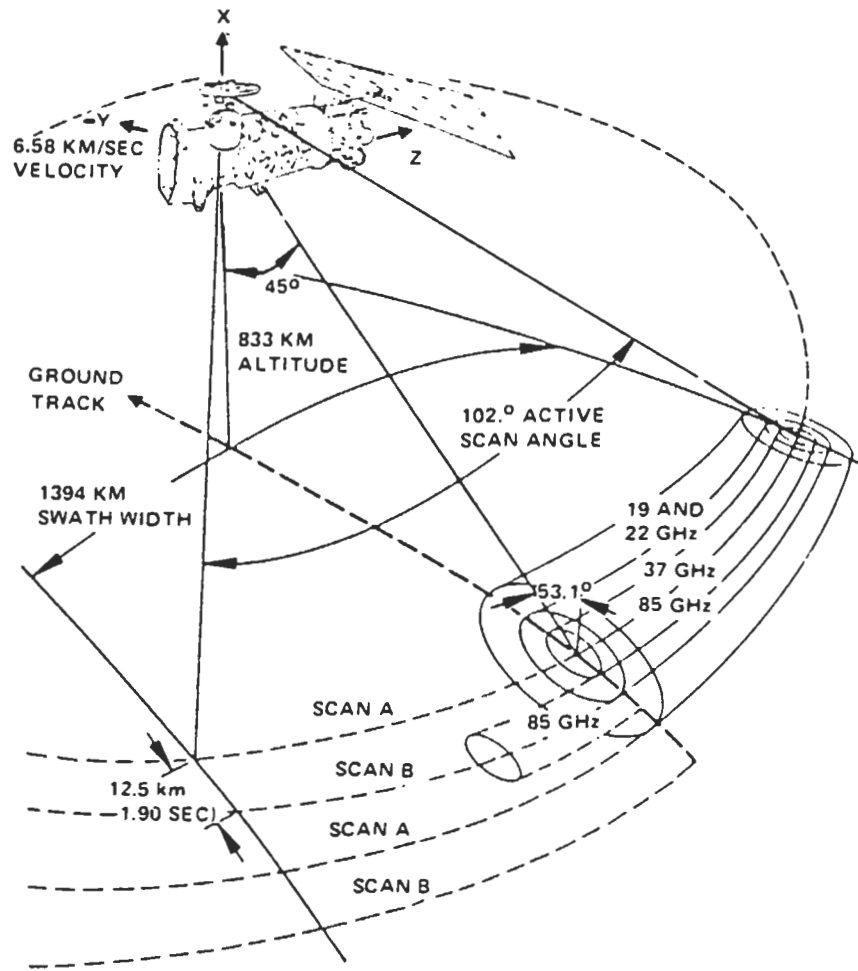


Figure 6: Instantaneous Field Of View, From [Hollinger et al.,1987]

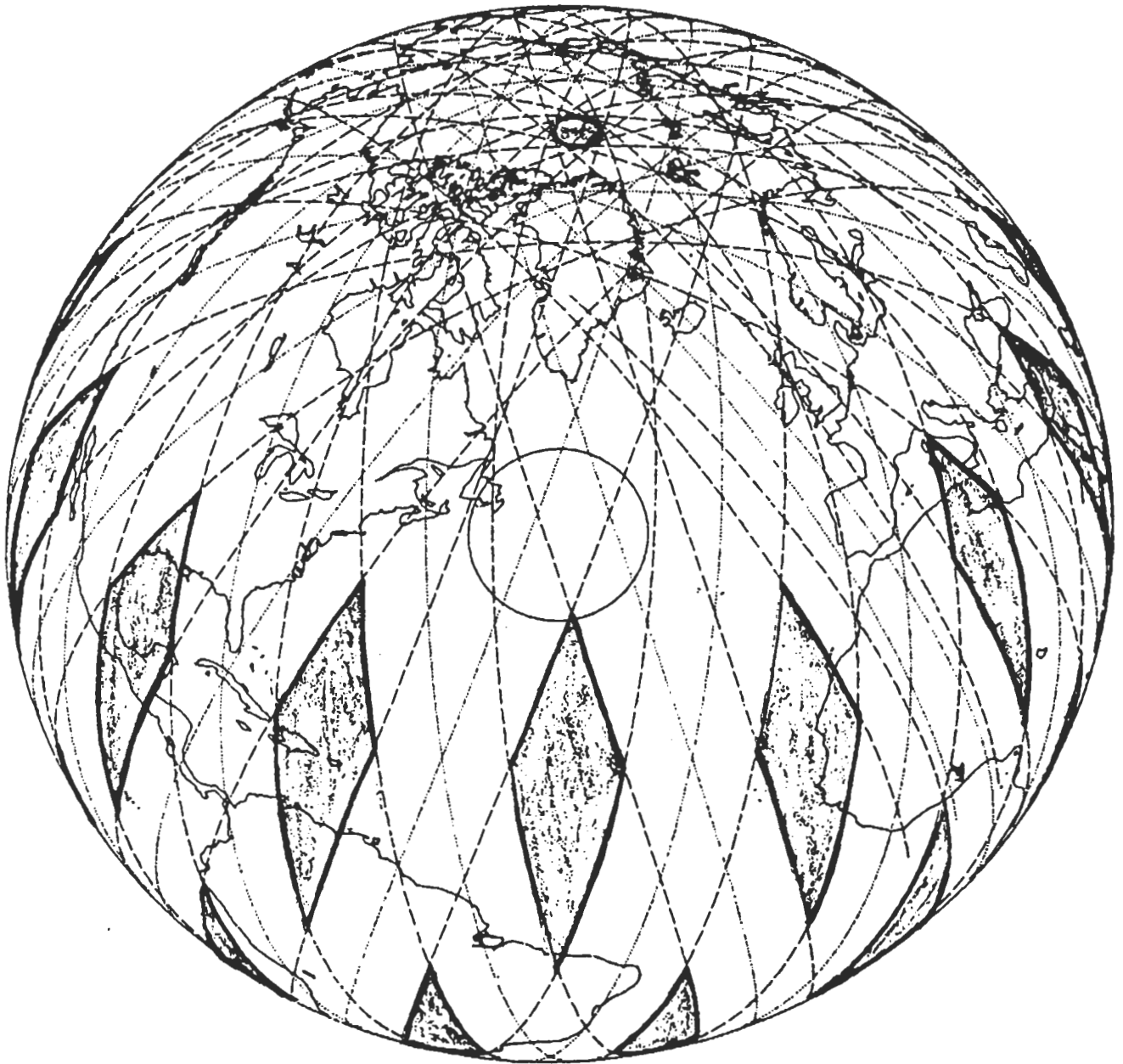


Figure 7: SSM/I Successive Orbits, From [Hollinger,1987]

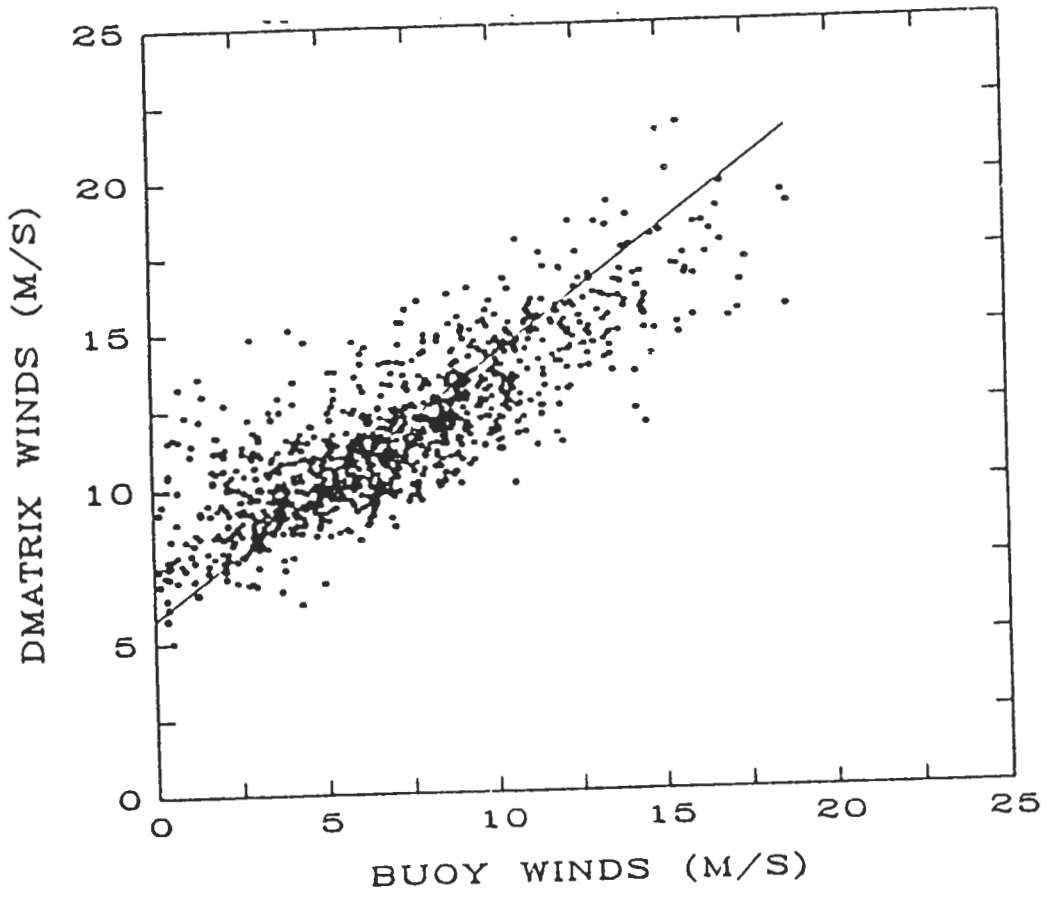


Figure 8 : Dmatrix Wind Speeds, From [Hollinger,1991]

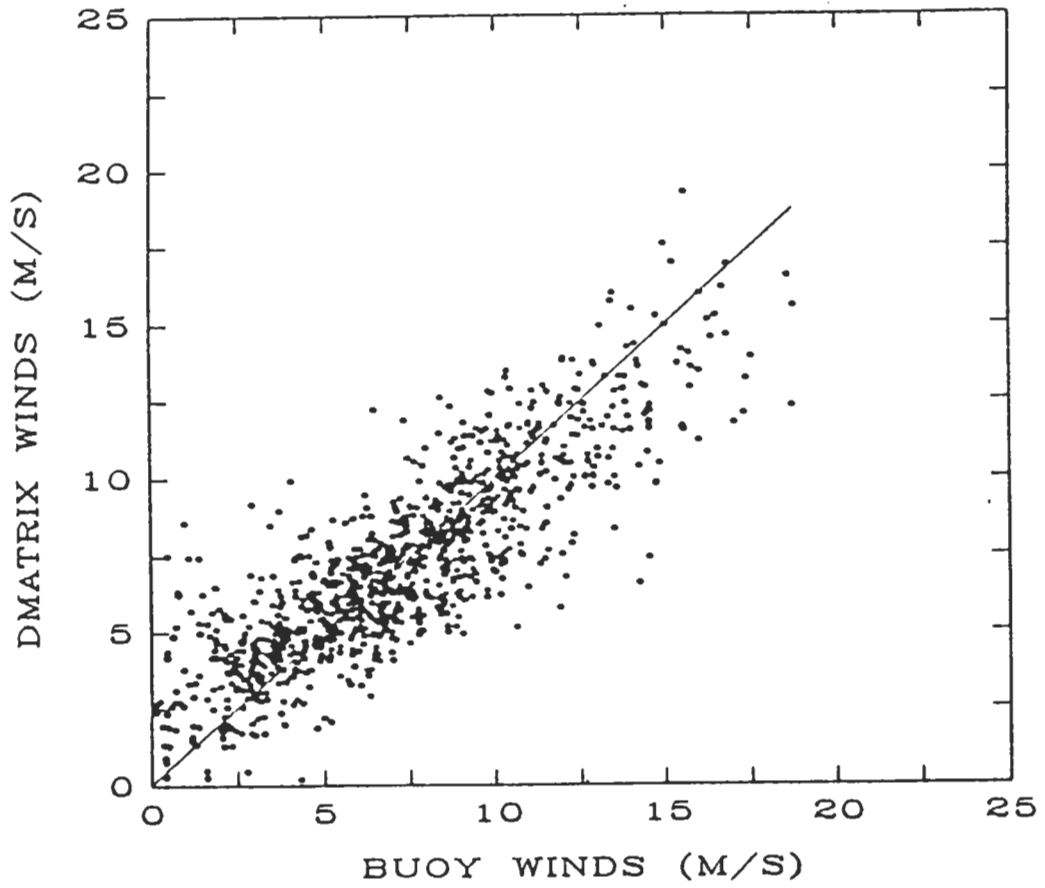


Figure 9: Dmatrix Wind Speeds, From [Hollinger,1991]

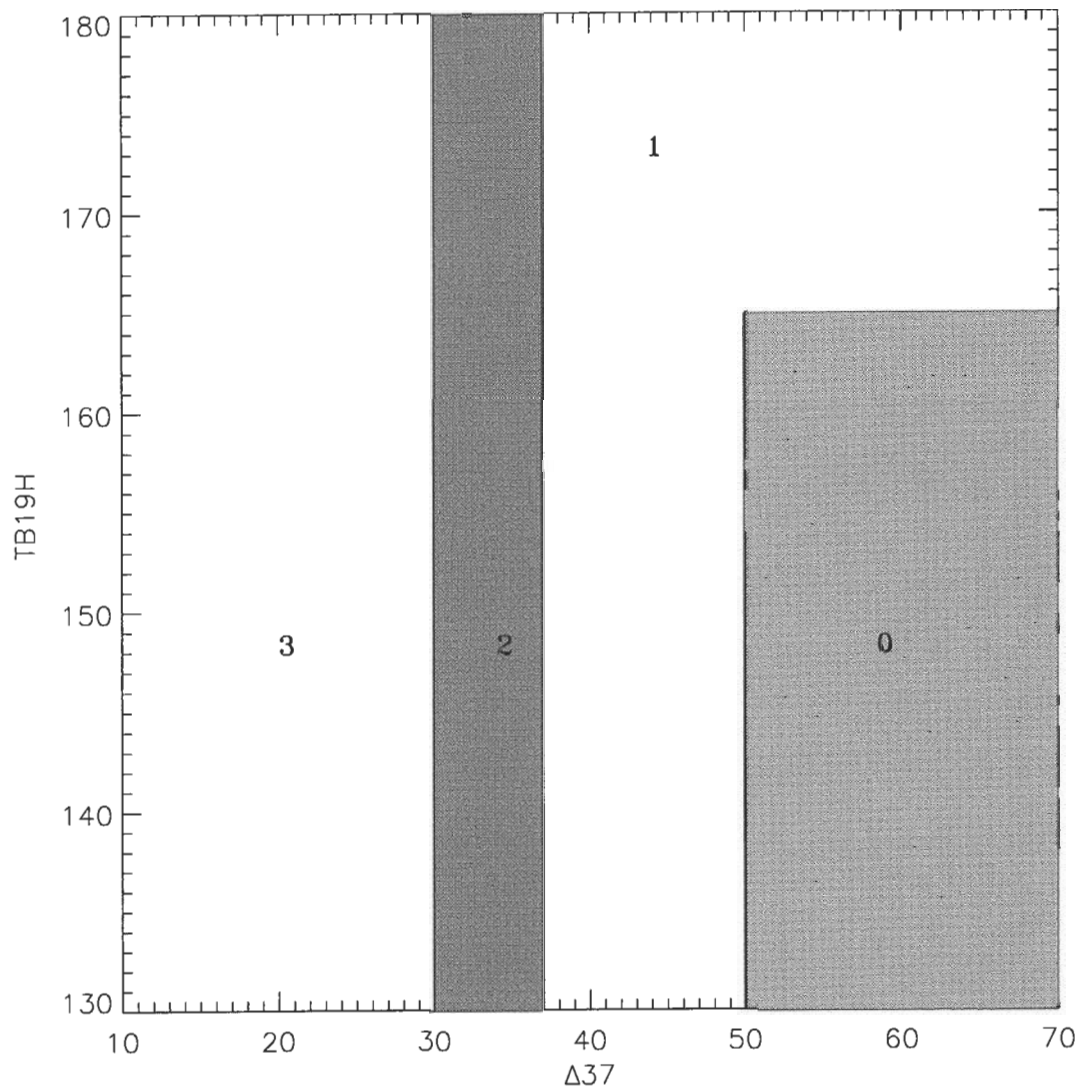


Figure 10 : Rain Flag Criteria

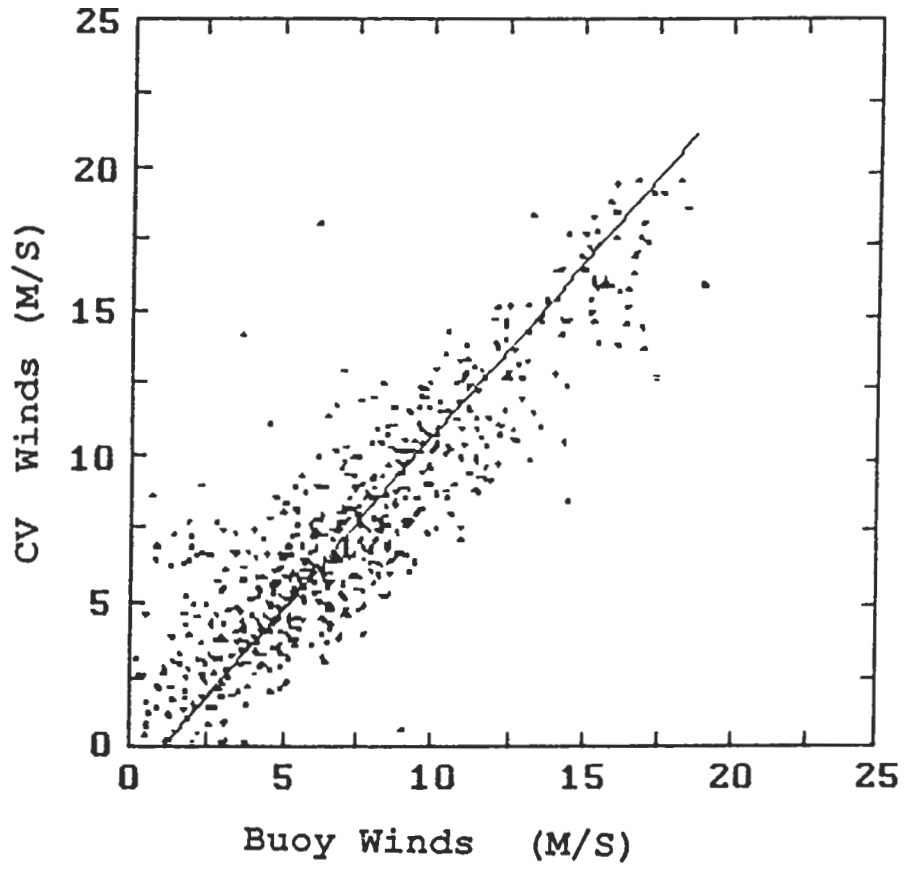


Figure 11: Calibration/Validation Algorithm, From [Hollinger,1991]

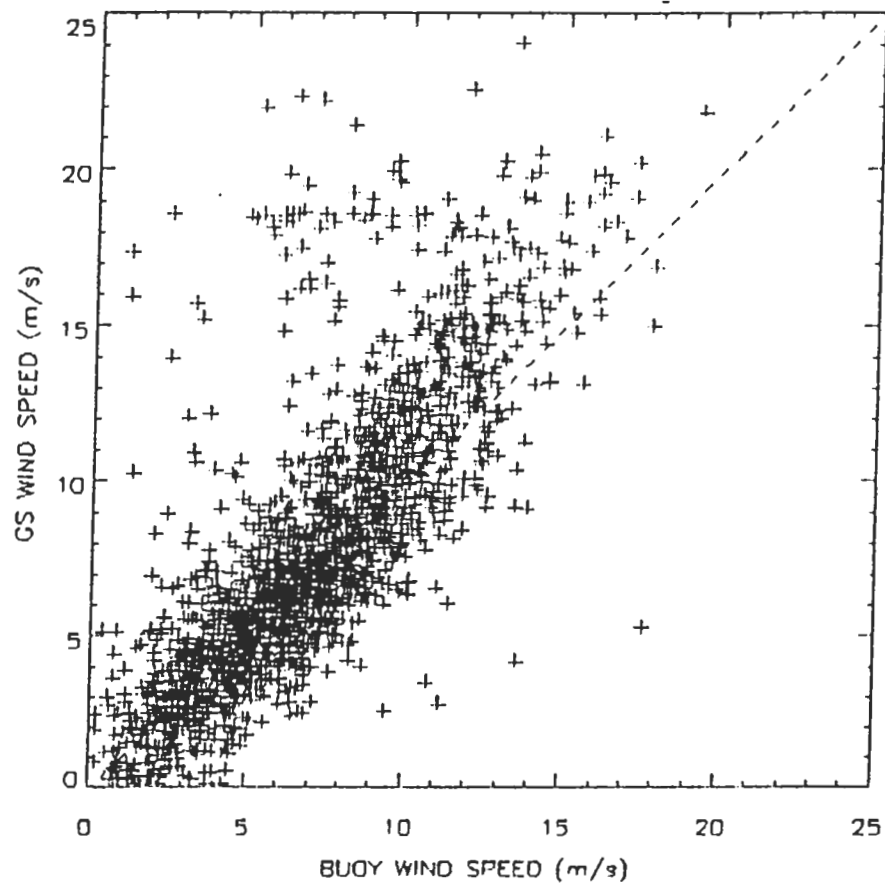


Figure 12: Goodberlet/Swift Algorithm, From [Krasnopolsky et al., 1994]

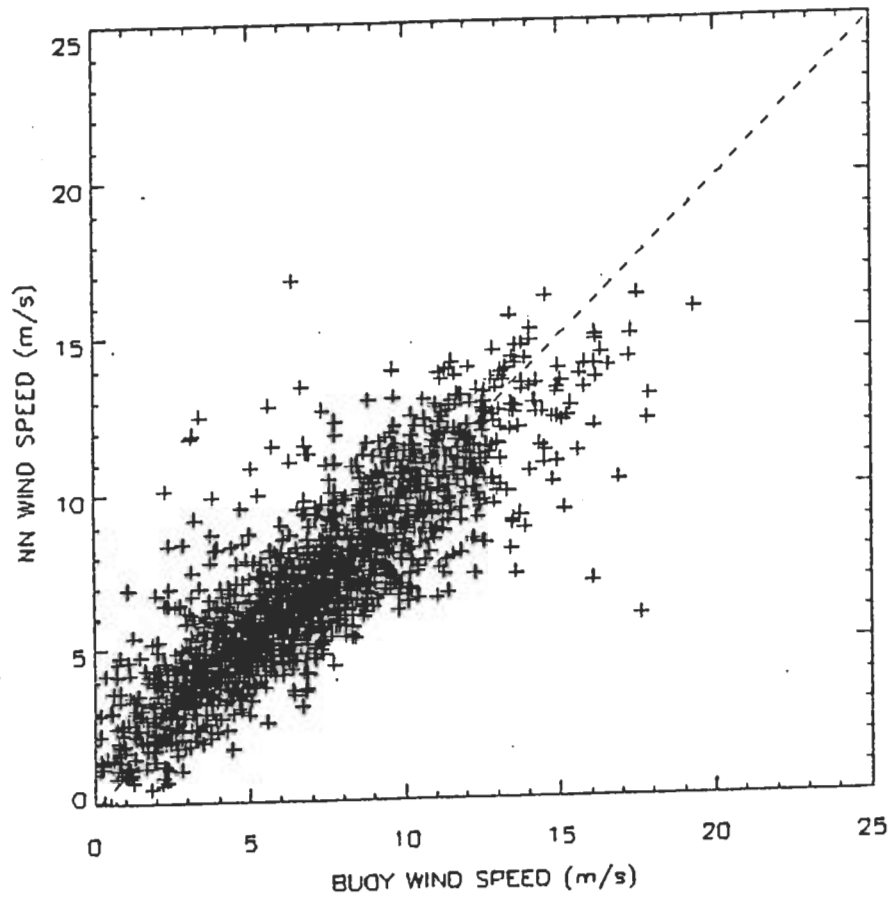


Figure 13: National Meteorological Center NN, From [Krasnopolsky et al., 1994]

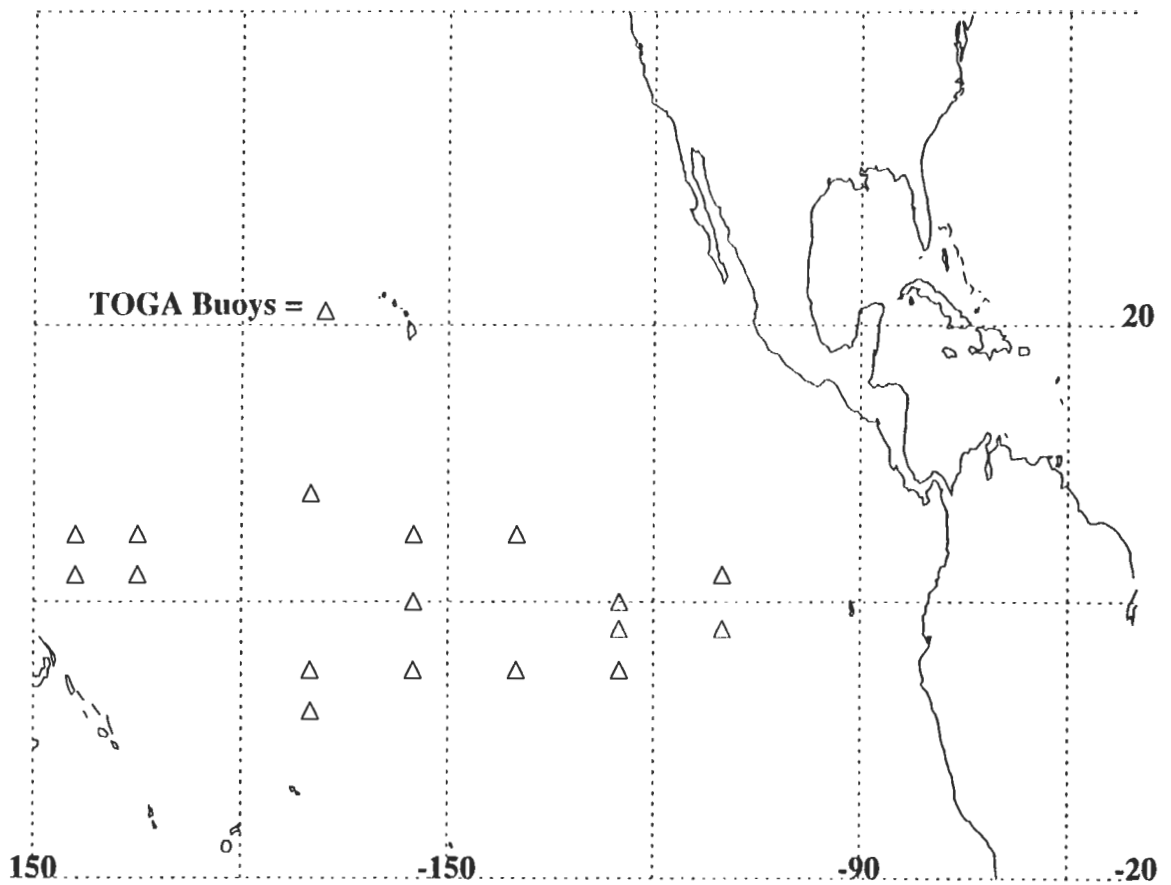


Figure 14: TOGA Buoys

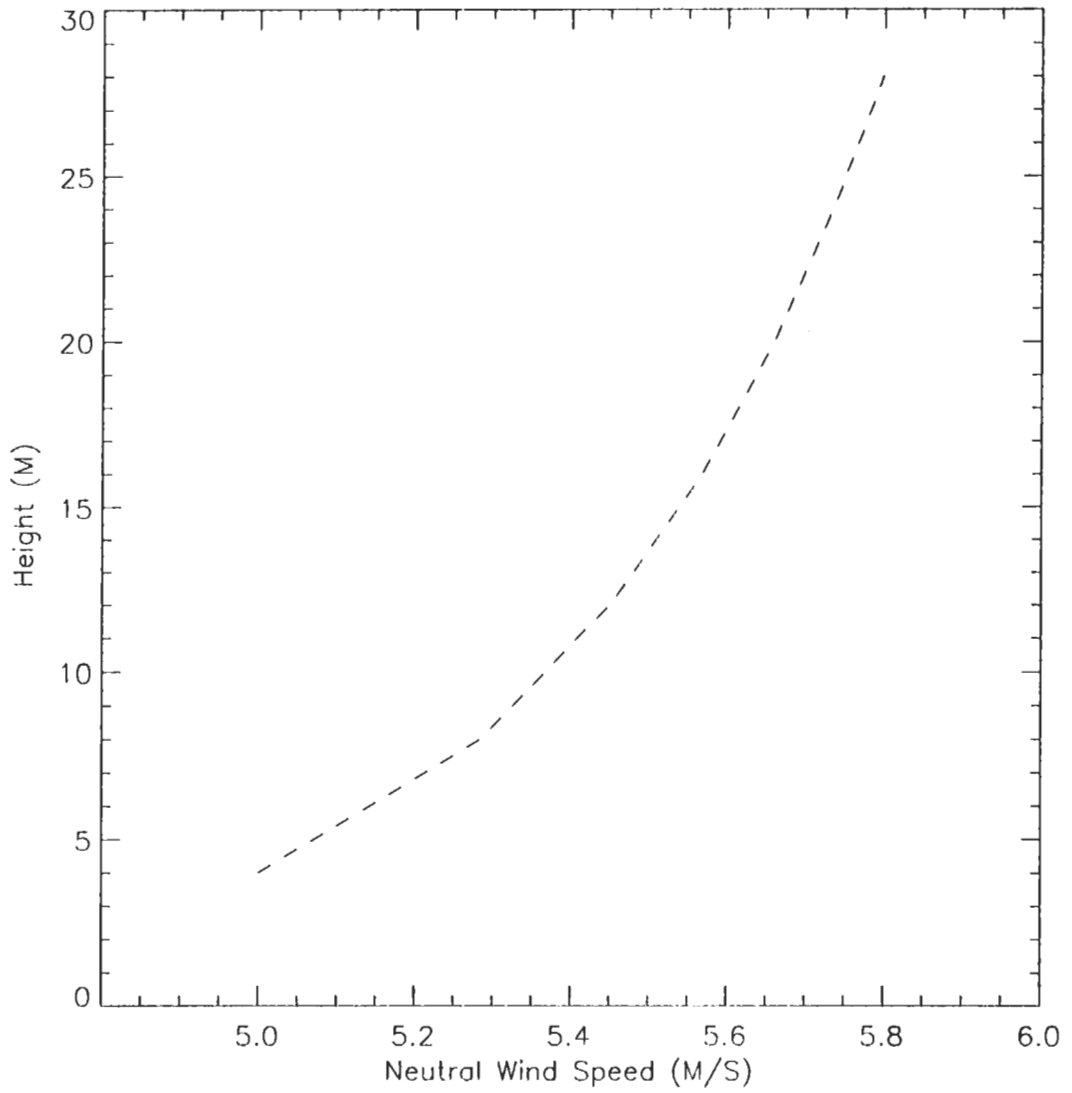


Figure 15: Neutral Wind vs Height over Ocean

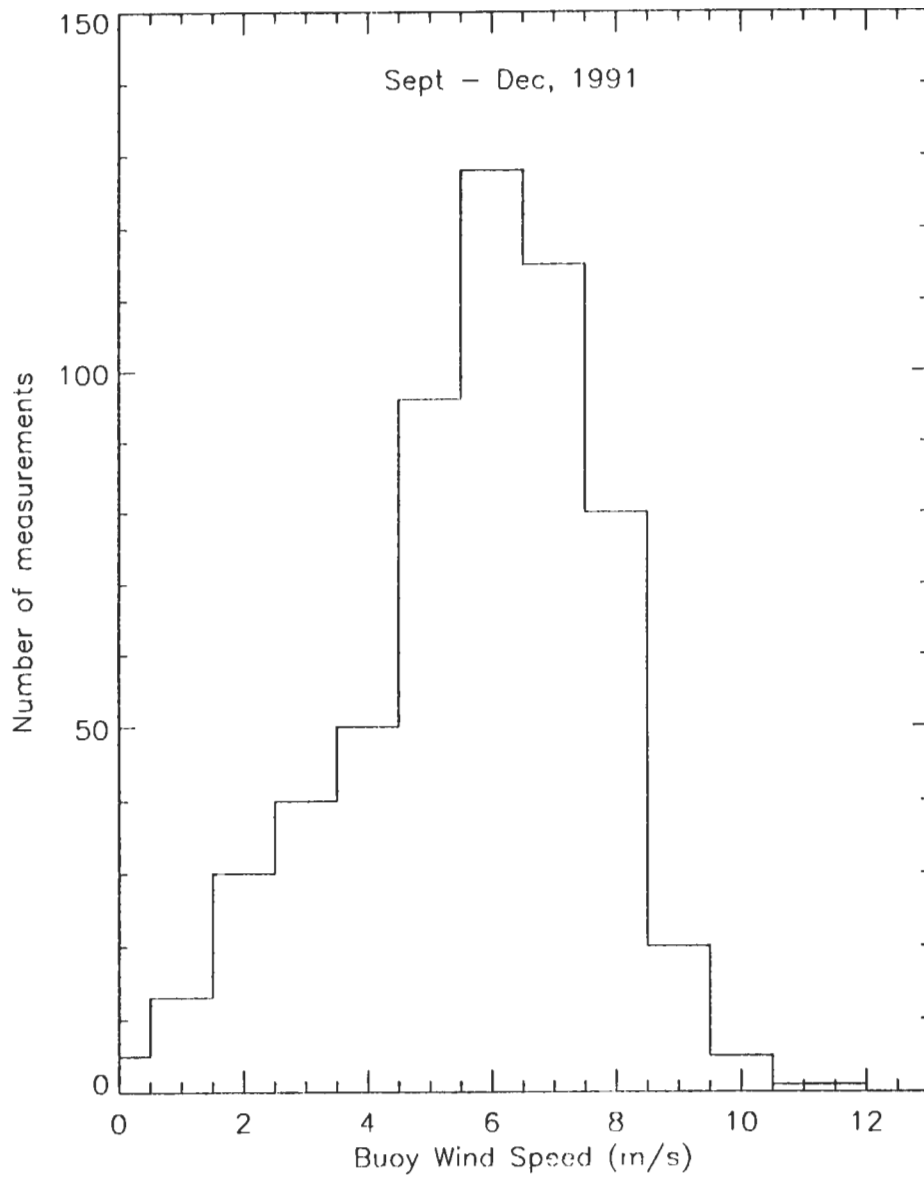


Figure 16: TOGA Wind Speed Distribution

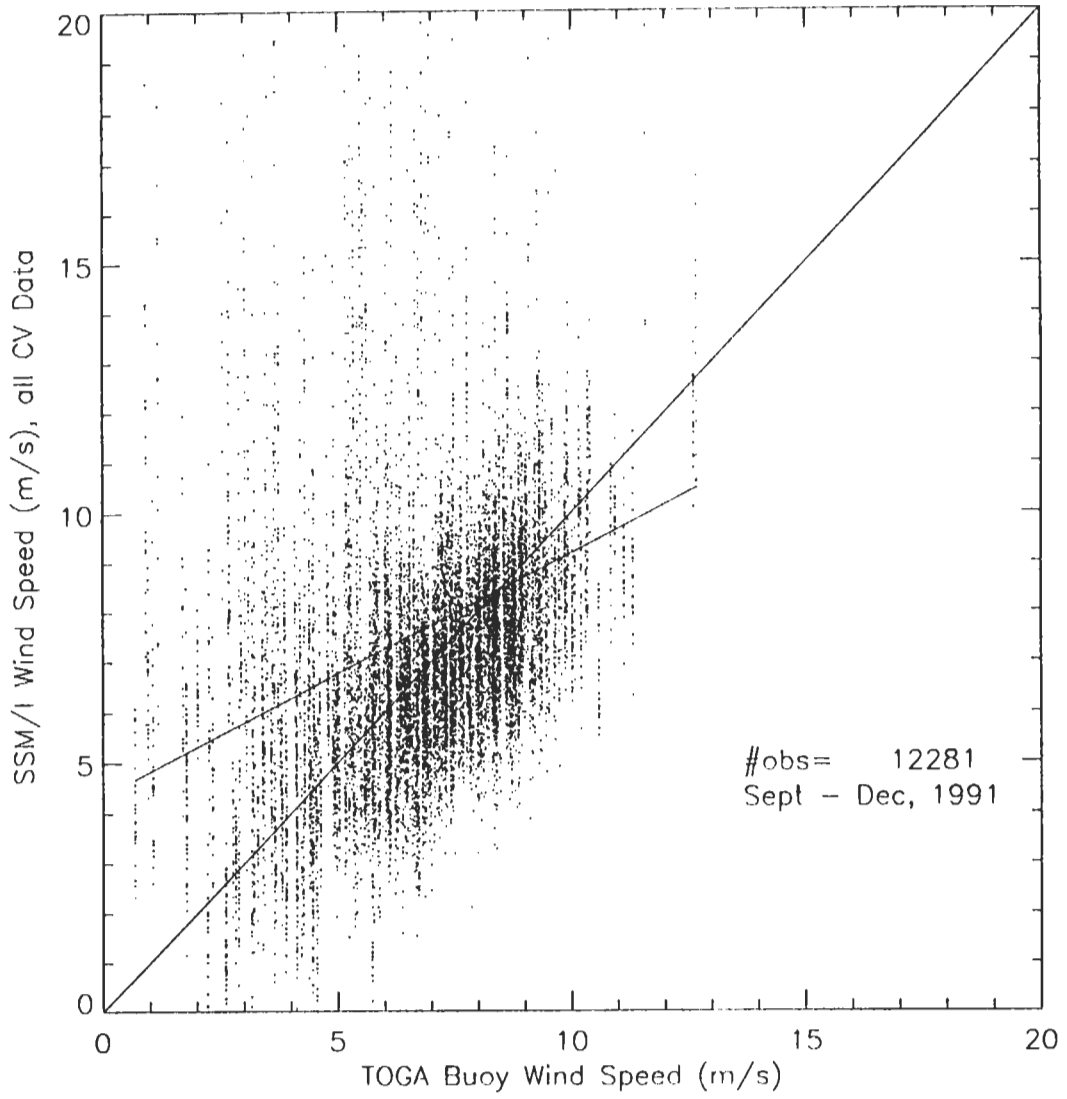


Figure 17: CV Wind Speed vs Buoy Wind Speed

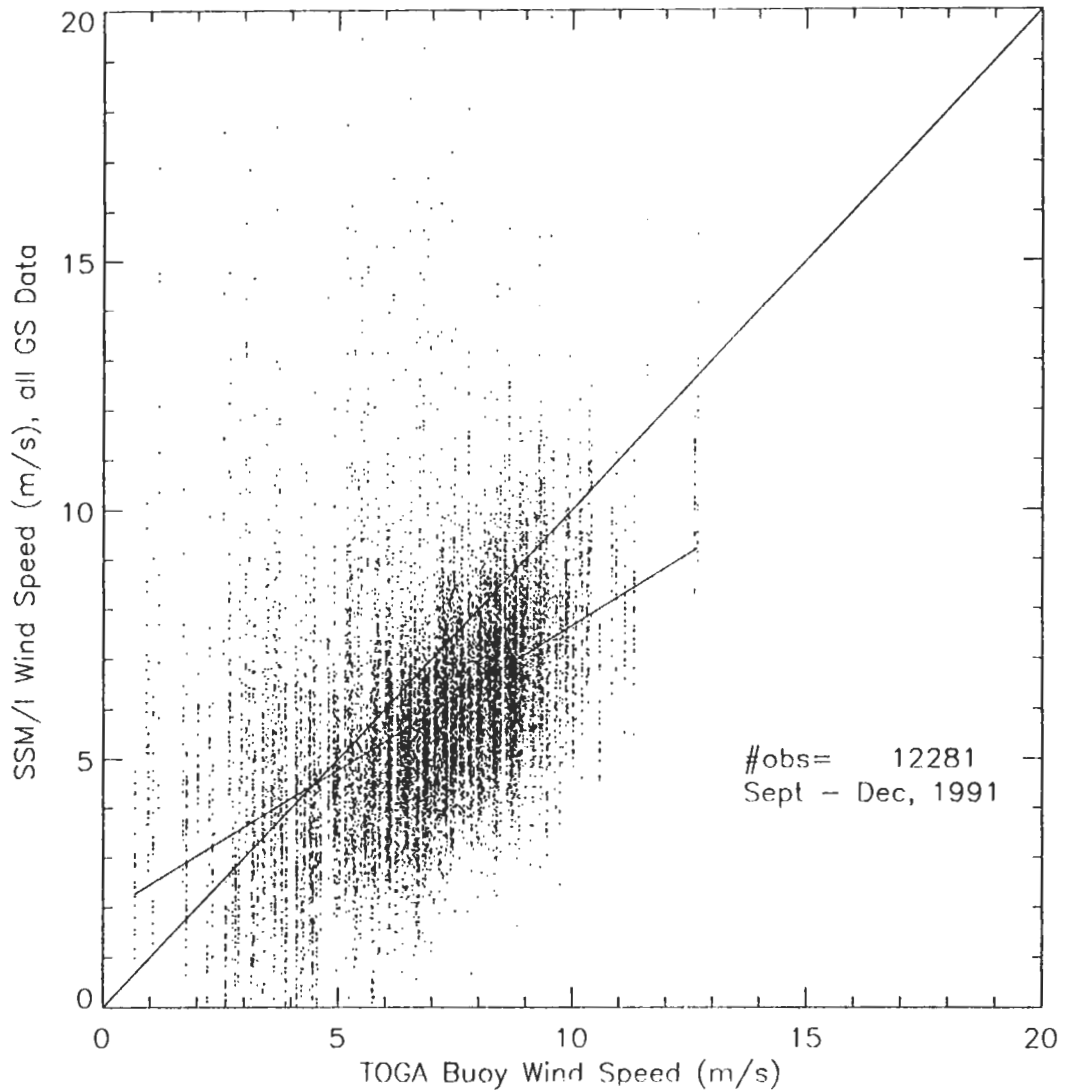


Figure 18: GS Wind Speed vs Buoy Wind Speed

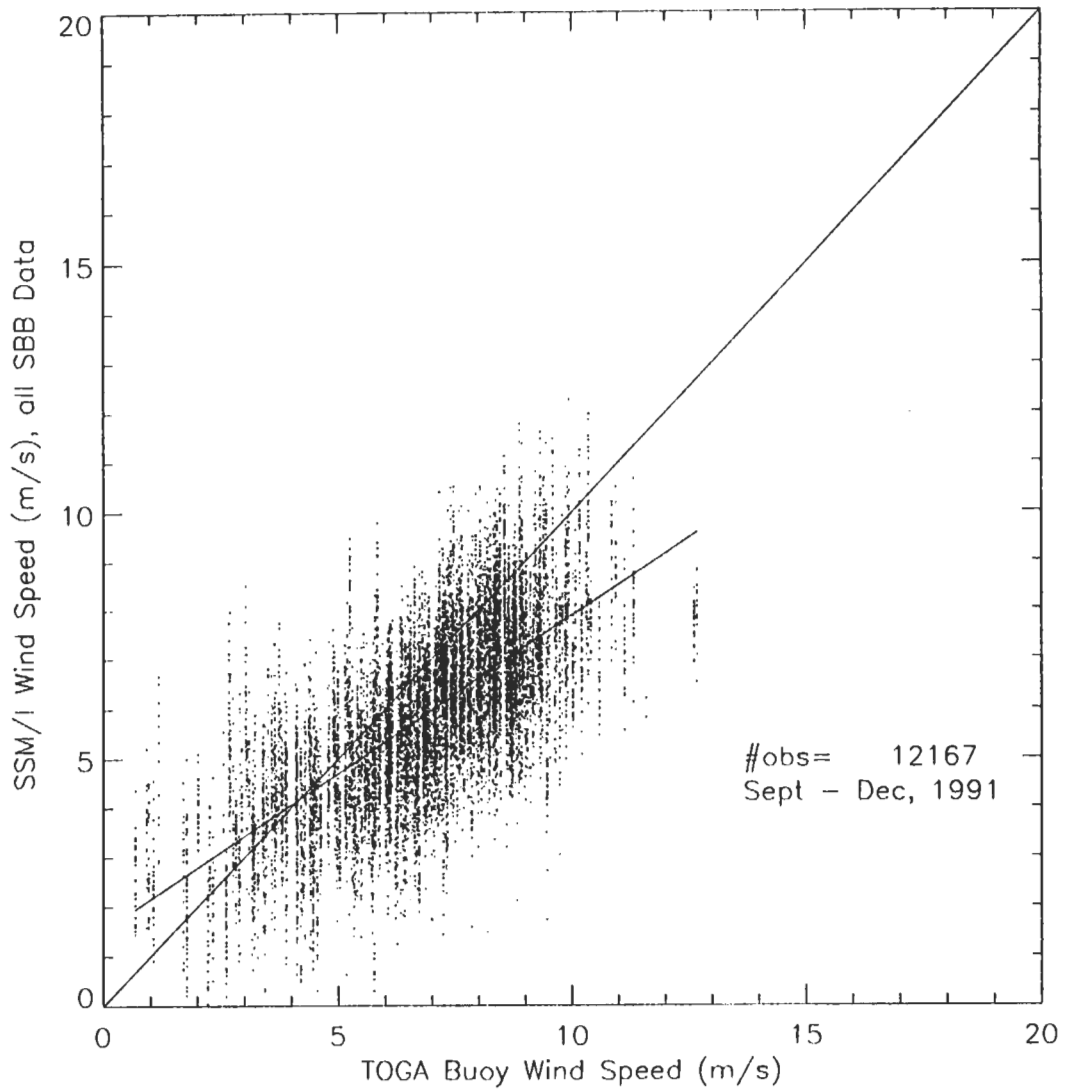


Figure 19: SBB wind Speed vs Buoy Wind Speed

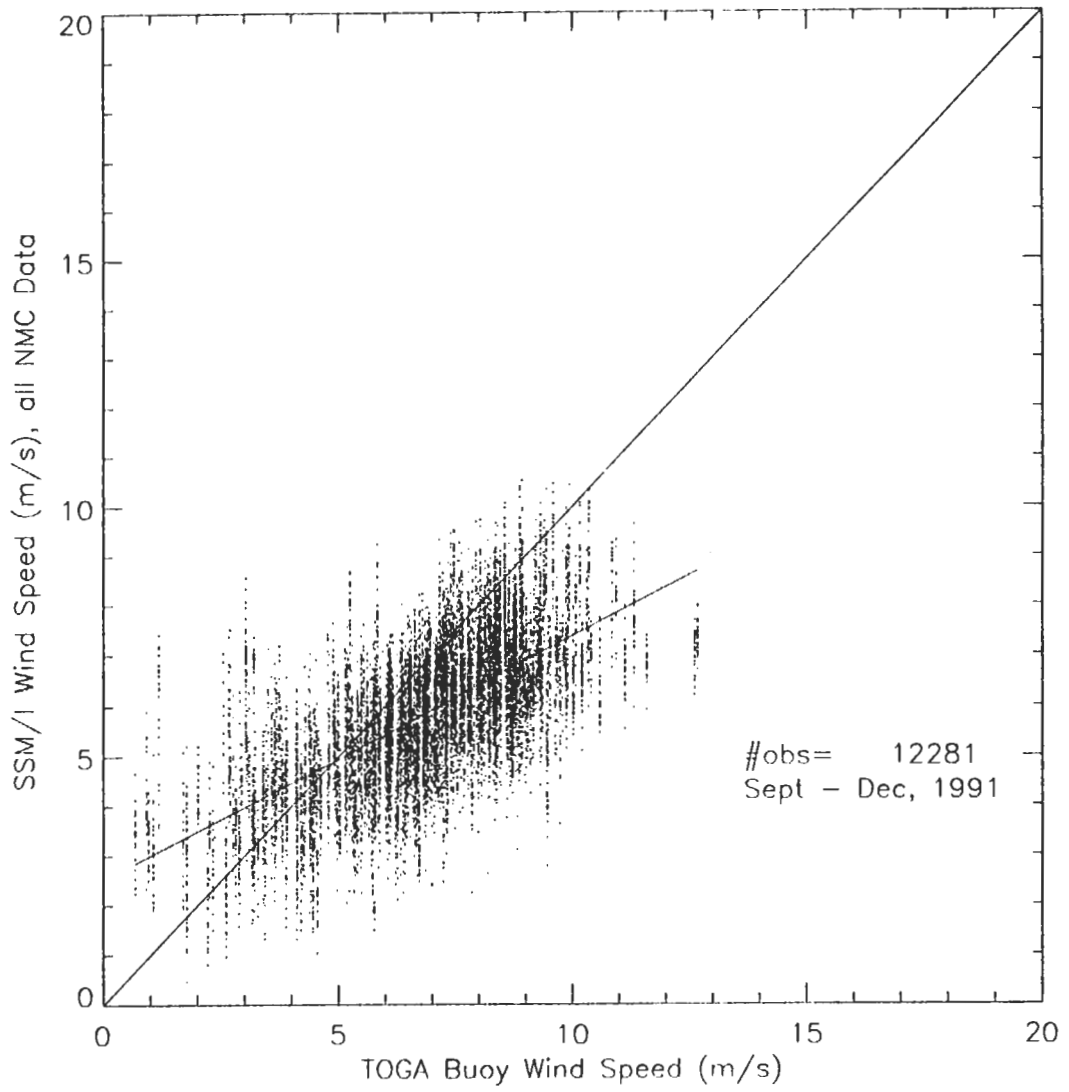


Figure 20 : NMC Wind Speed vs Buoy Wind Speed

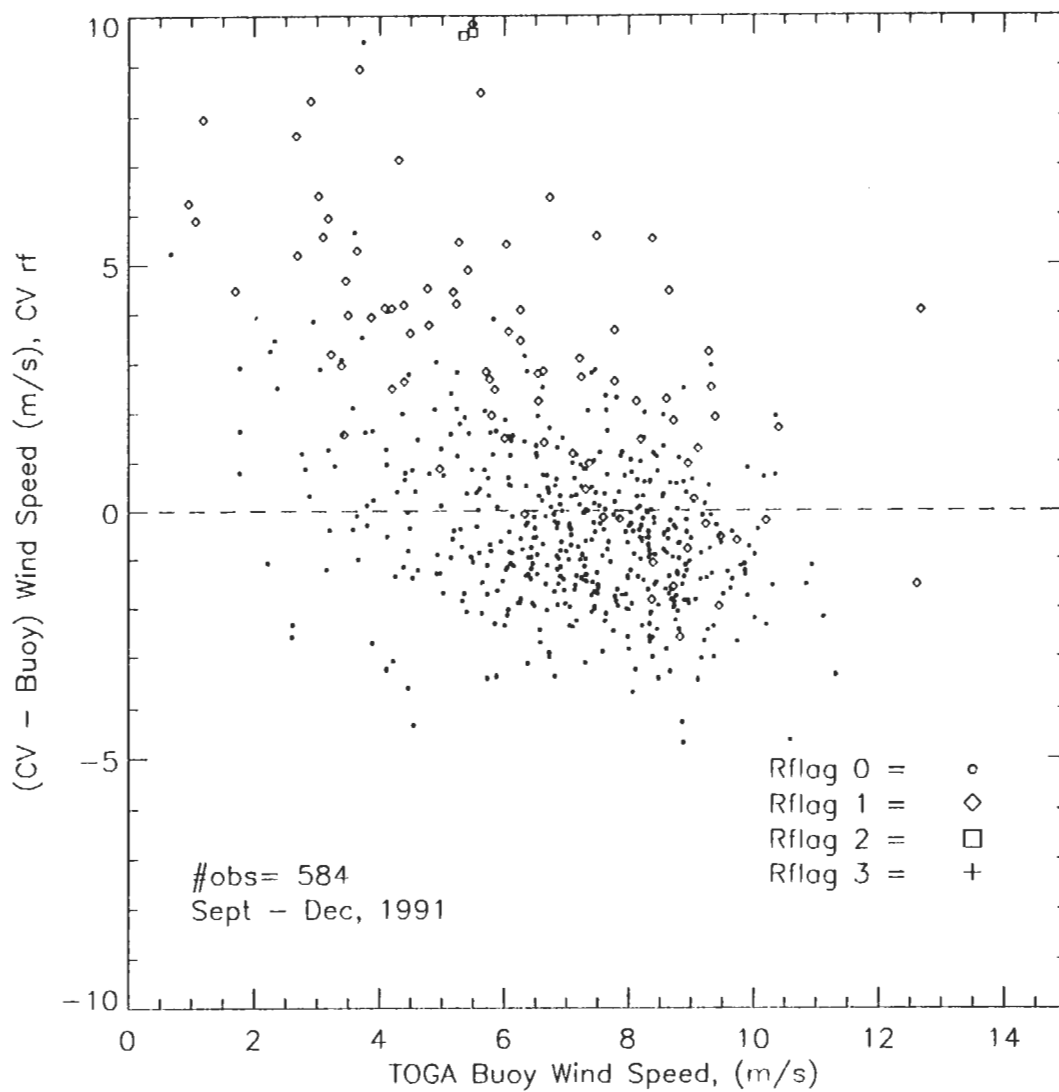


Figure 21 : (CV - Buoy) Wind Speed vs Buoy Wind Speed

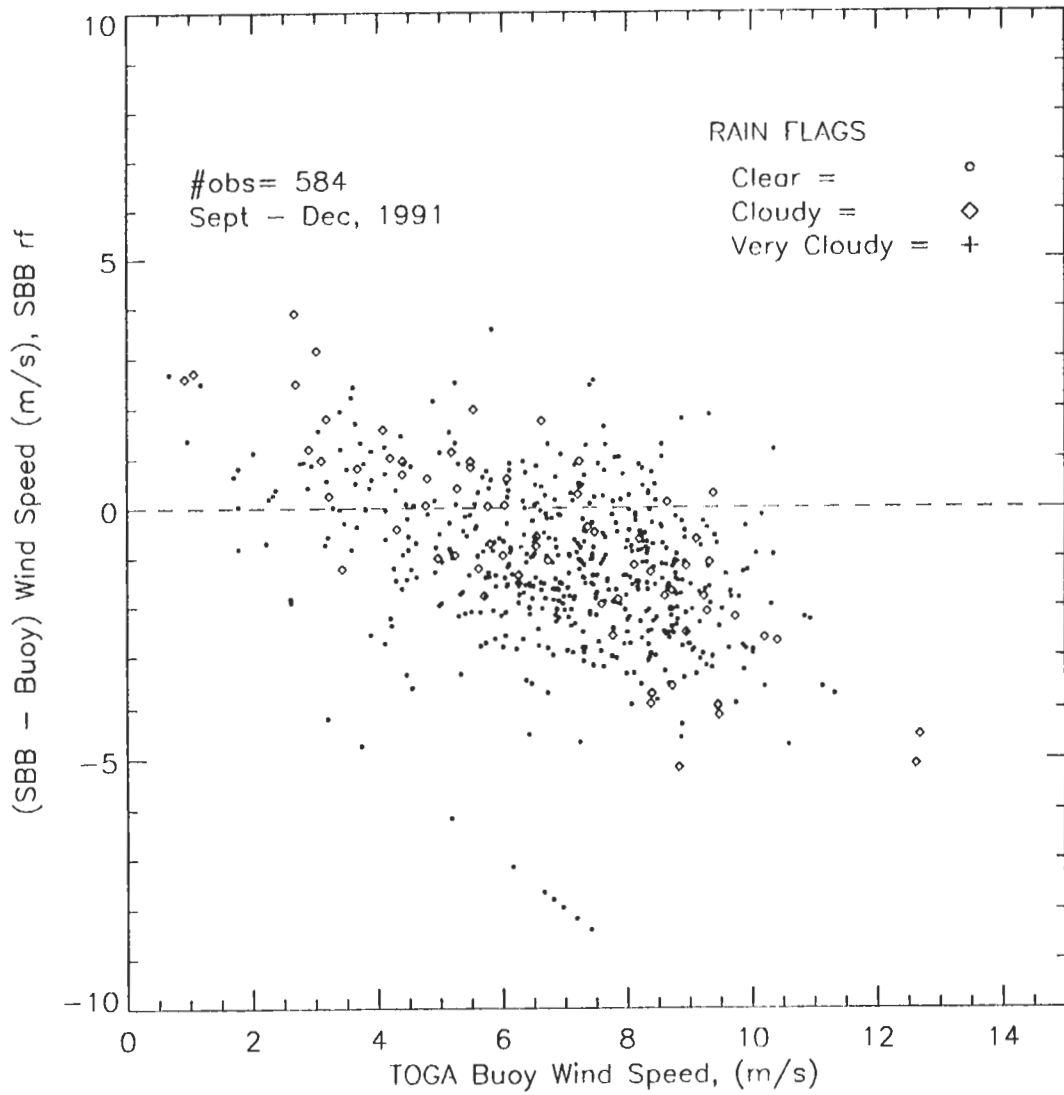


Figure 22 : (SBB - Buoy) Wind Speed vs Buoy Wind Speed

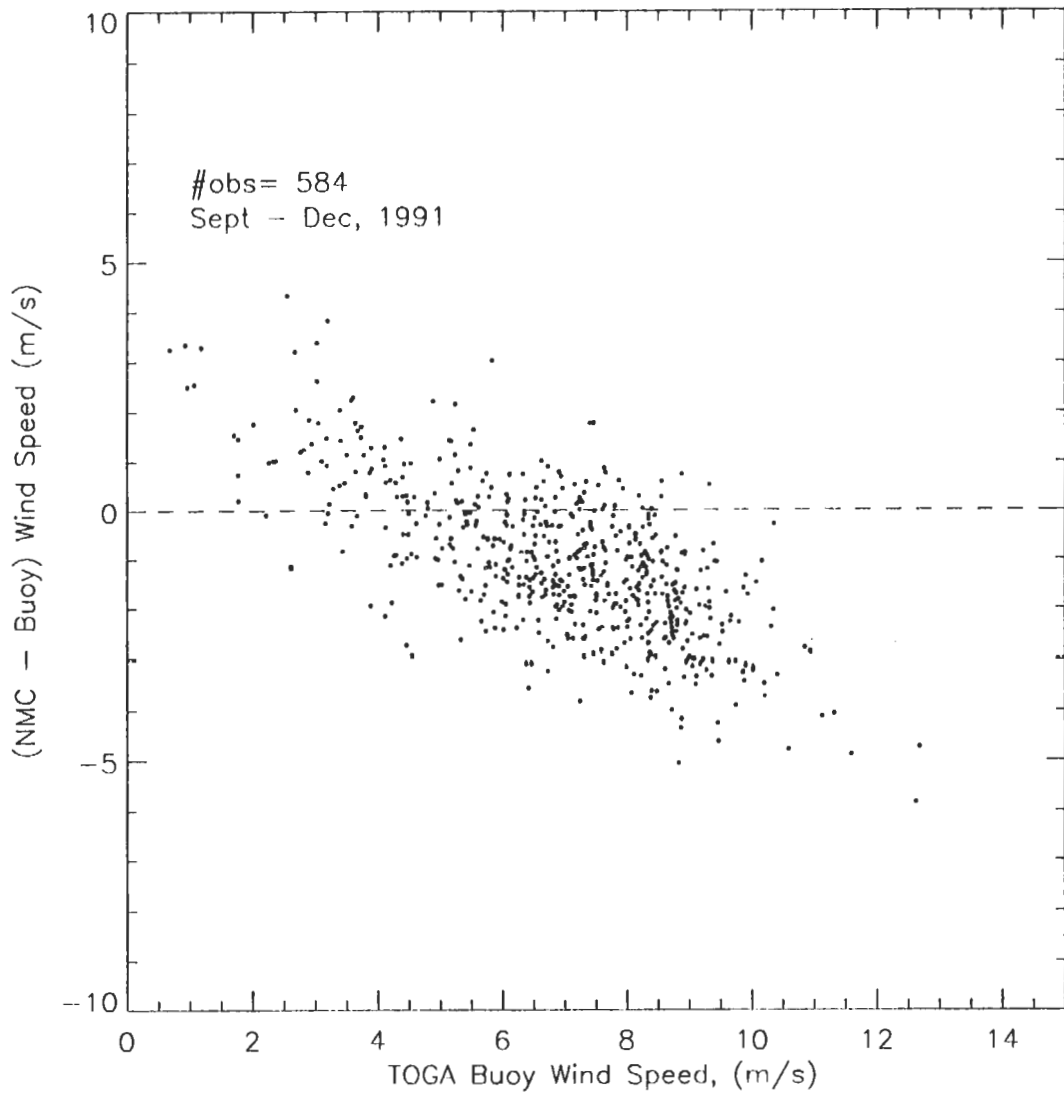


Figure 23 : (NMC - Buoy) Wind Speed vs Buoy Wind Speed

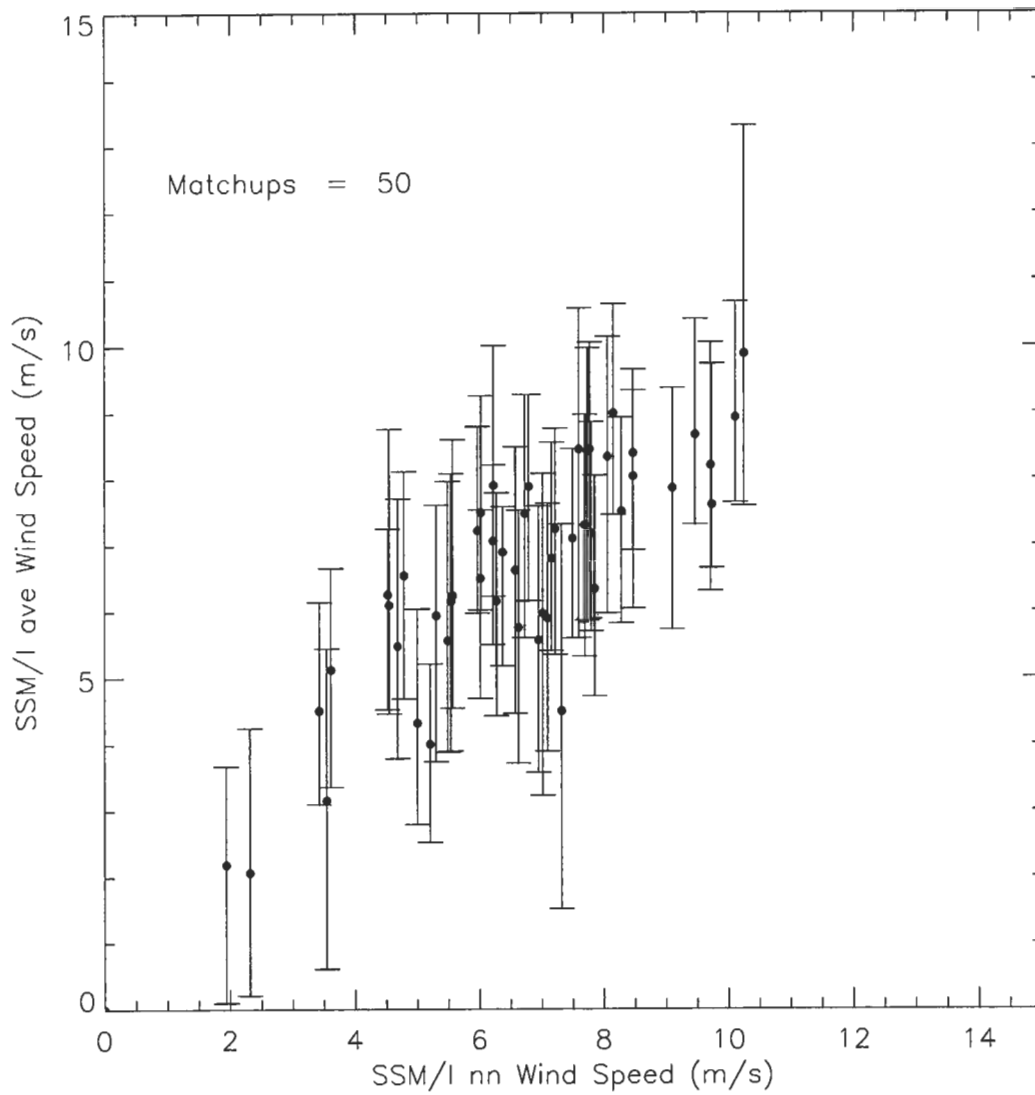


Figure 24 : Comparison of SSM/I nn and ave wind speed retrievals with associated range of values for a typical buoy matchup

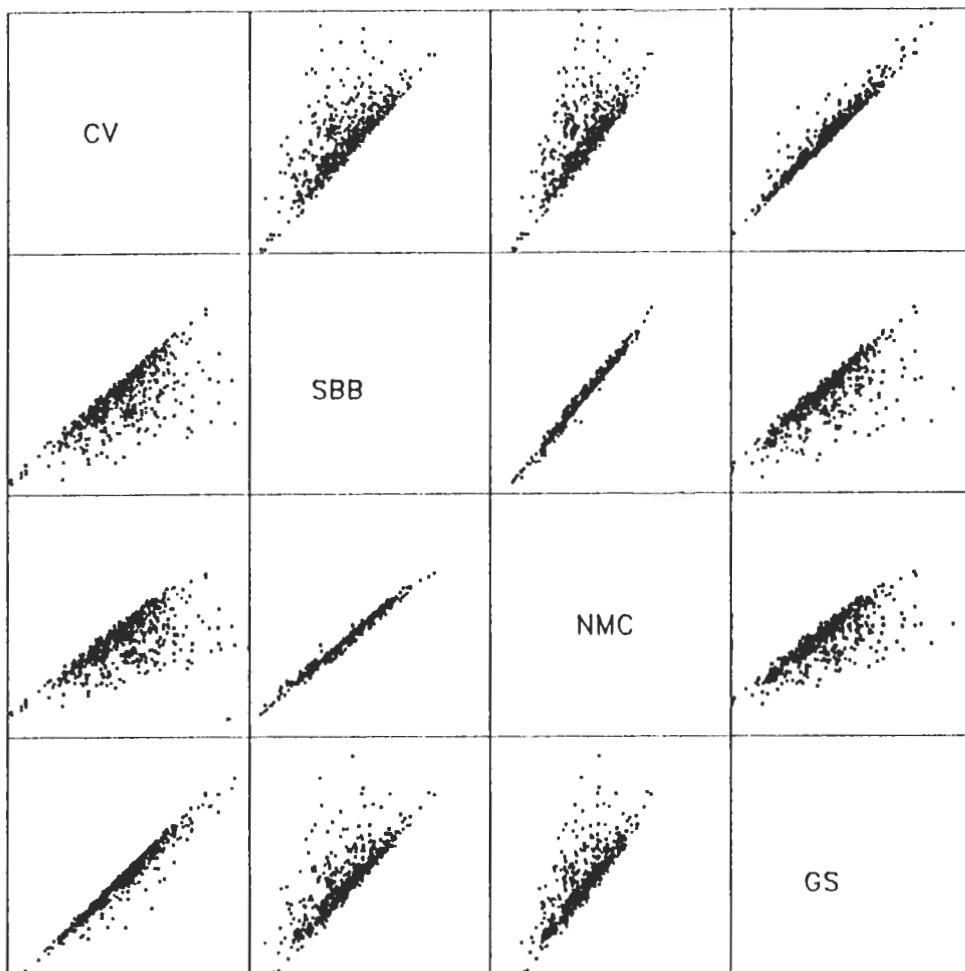


Figure 25 : Comparison of Wind Speed Retrieval Methods
DMSP SSM/I, Sept - Dec, 1991

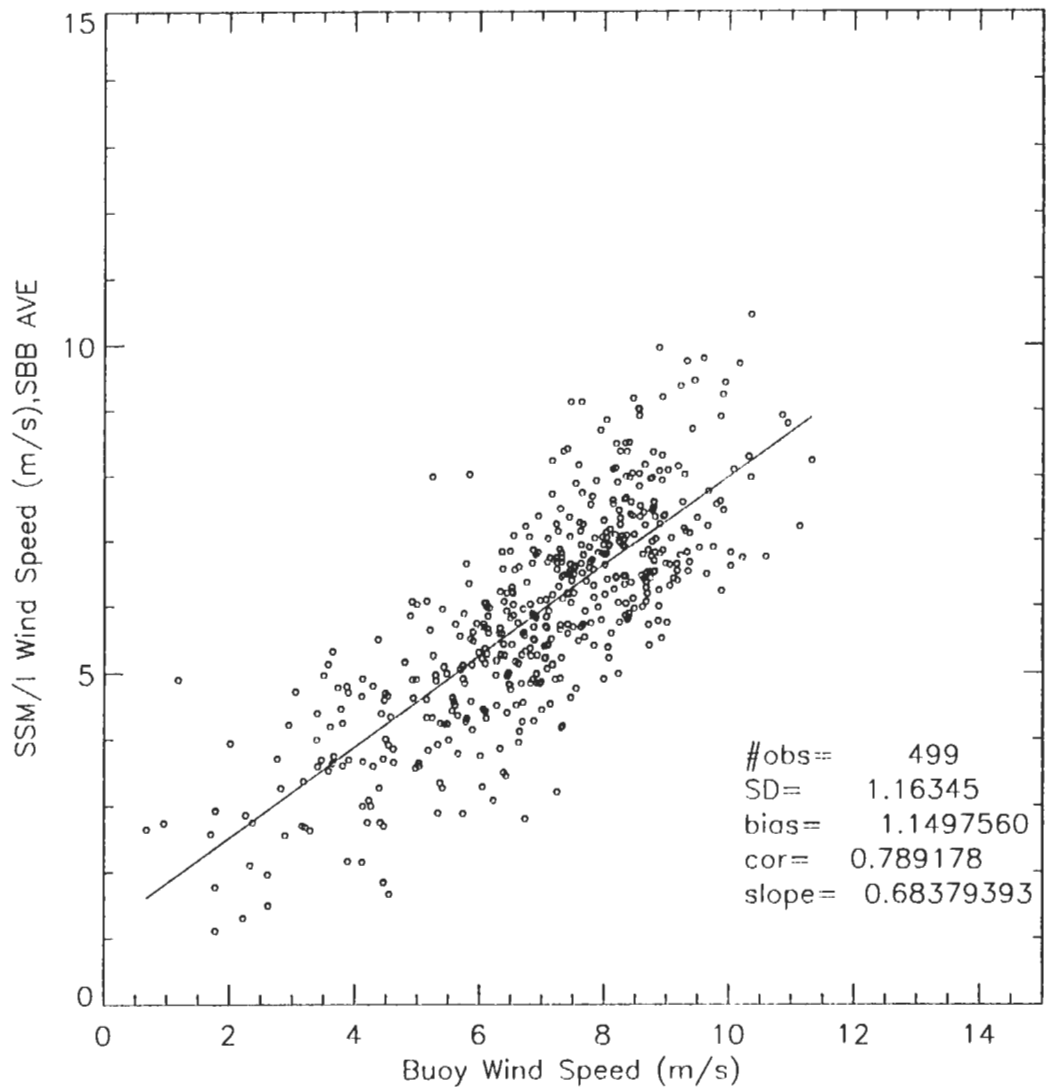


Figure 26 : SBB Wind Speed vs Buoy Wind Speed, Rain Flag 0

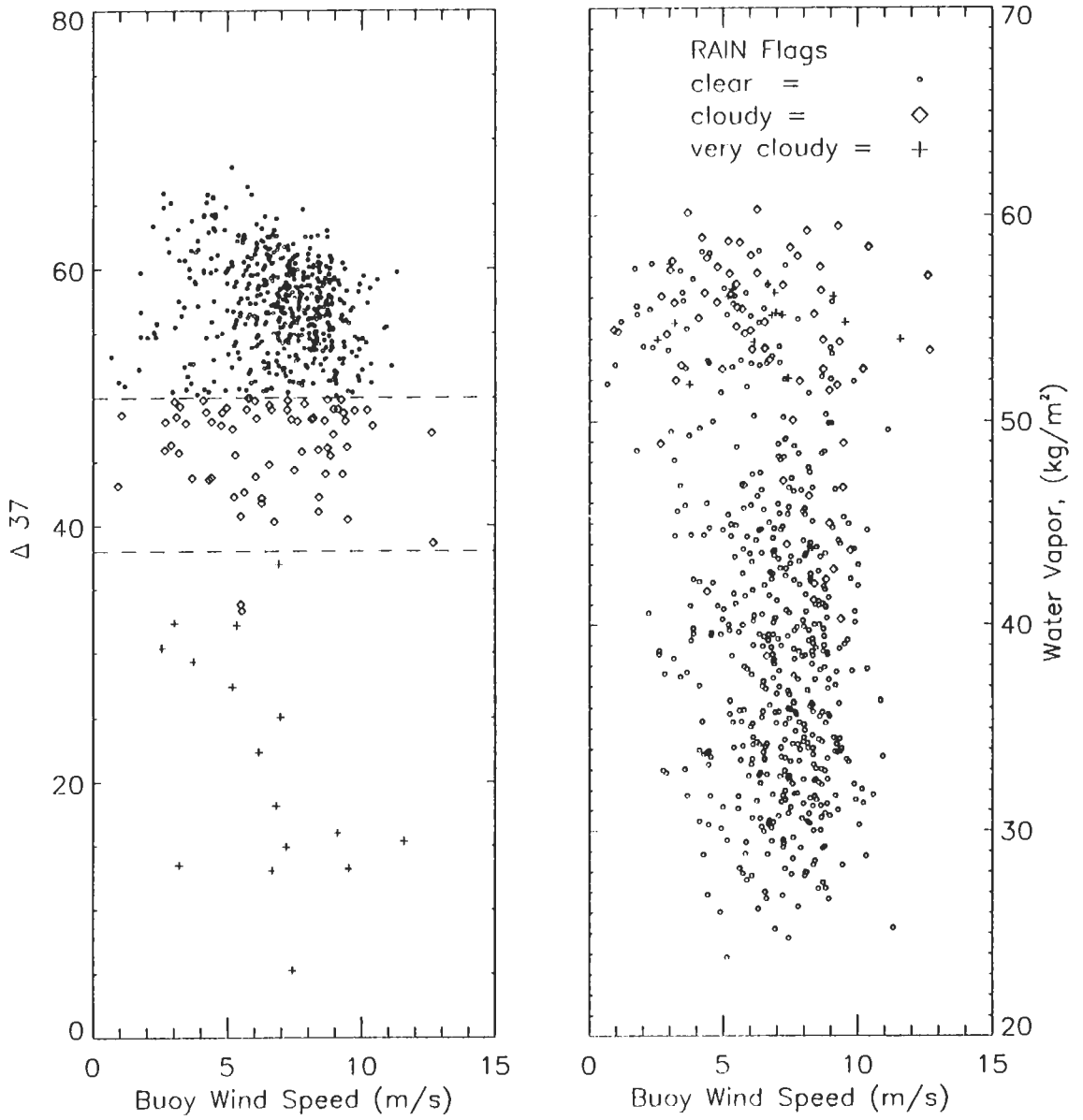


Figure 27 : Partitioning of SSM/I Wind Speeds

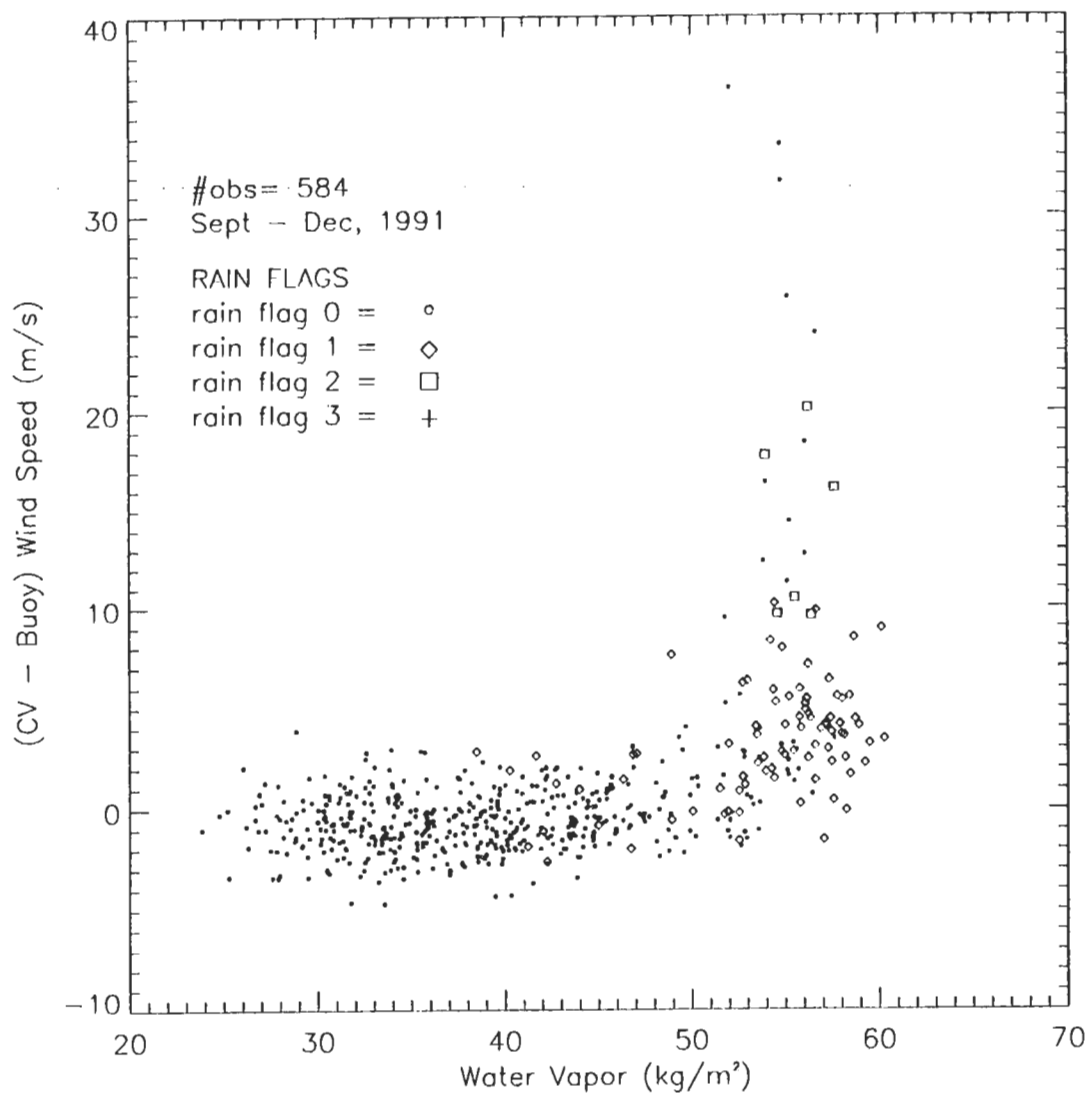


Figure 28 : (CV - Buoy) Wind Speed vs Water Vapor

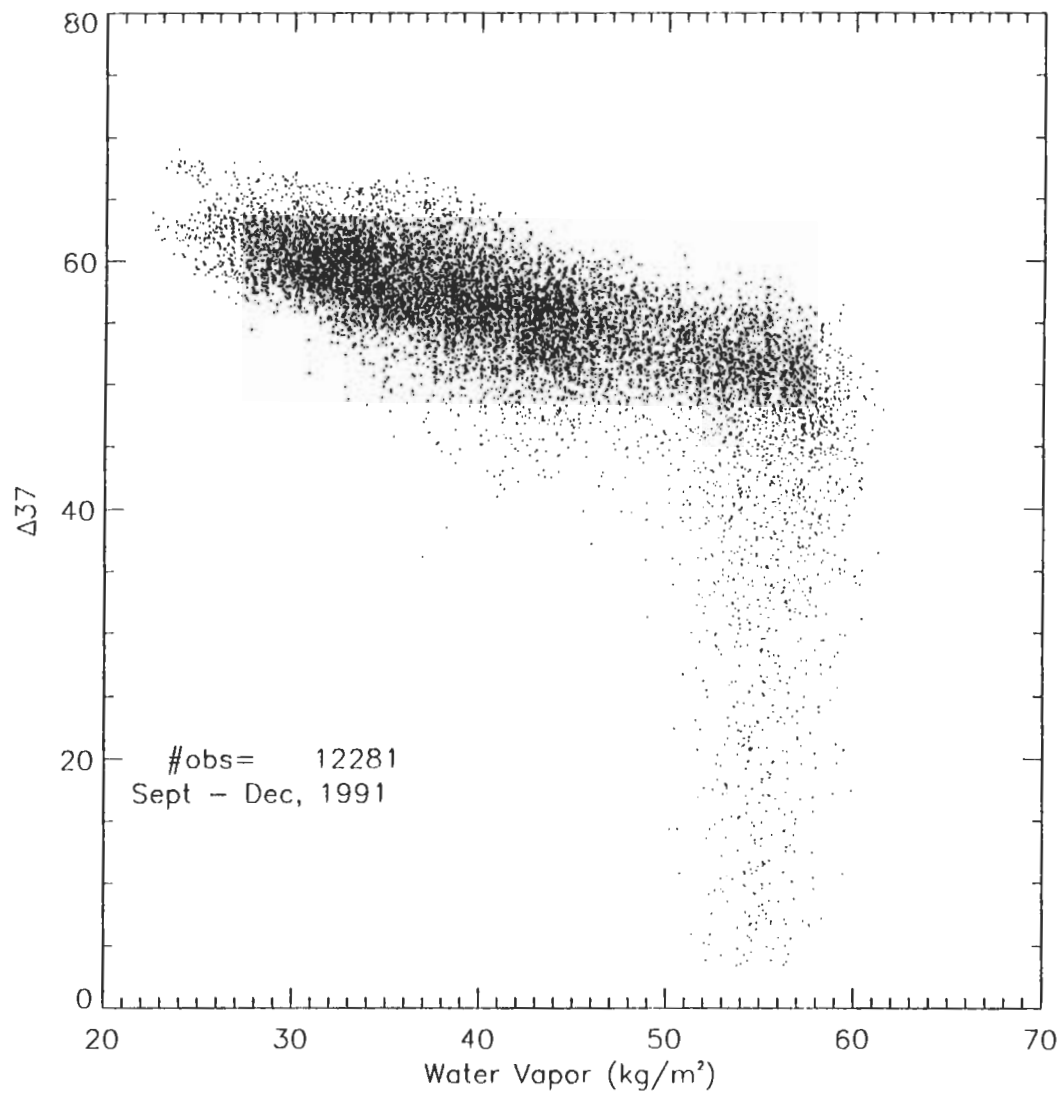


Figure 29 : T_{B37} vs Water Vapor

APPENDIX B: TABLES

TOGA BUOYS USED FOR SSM/I COMPARISONS			
BUOY I.D.	LATITUDE	LONGITUDE (E)	ZONE
90001	02.0 N	250.0	Equatorial
90002	02.0 S	250.0	Equatorial
90003	00.0	235.0	Equatorial
90004	02.0 S	235.0	Equatorial
90005	05.0 S	235.0	Equatorial
90006	05.0 N	220.0	Equatorial
90008	05.0 S	220.0	Equatorial
90009	05.0 N	205.0	Equatorial
90010	00.0	205.0	Equatorial
90011	05.0 S	205.0	Equatorial
90012	08.0 N	190.0	Equatorial
90013	05.0 S	190.0	Equatorial
90014	08.0 S	190.0	Equatorial
90015	05.0 N	156.0	Equatorial
90016	02.0 N	156.0	Equatorial
90018	05.0 N	165.0	Equatorial
90019	02.0 N	165.0	Equatorial

Table 1: TOGA Buoys

	CV (nn)	CV (ave)	CV (Wave)	GS (nn)	GS (ave)	GS (Wave)
SD	1.57	1.32	1.33	1.55	1.23	1.24
BIAS	1.73	1.84	1.78	.493	.581	.533
COR	.646	.718	.720	.660	.755	.753
SLOPE	.686	.682	.688	.707	.704	.710

	SBB (nn)	SBB (ave)	SBB (Wave)	NMC (nn)	NMC (ave)	NMC (Wave)
SD	1.37	1.16	1.14	1.30	1.12	1.13
BIAS	.942	1.15	.951	1.82	1.83	1.81
COR	.712	.789	.788	.705	.787	.783
SLOPE	.706	.684	.711	.576	.581	.581

Table 2: Wind Speed Retrieval Performance

Frequency (GHz)	Purpose	Used this Study
19.3V 19.3H	atmospheric window sea surface brightness temperature retrieval	yes
22.2V	atmospheric water vapor indicator(emissivity)	yes
37.0V 37.0H	atmospheric window difference in polarization used to generate rain flags	yes
85.5V 85.5H	higher spatial resolution	no

Table 3: SSM/I Frequencies

LIST OF REFERENCES

- Dawson, M.S. and A.K. Fung, "Neural Networks and the applications to parameter retrieval and classification," *IEEE Geoscience and Remote Sensing Society News Letter*, pp. 6 -14, 1993.
- Fretag, H.P., M.J. McPhaden, and A.J. Shepard, "Comparison of equatorial winds measured by cup and propeller anemometers," *Journal of Atmospheric and Oceanic Technology*, vol 6, pp. 327 -332, 1989.
- Gloresen, P., D.J. Cavalieu, T.C. Chang, T.T. Wilheit, W.J. Campell, O.M. Johannessen, K.B. Katsaros, K.F. Kunzi, D.B. Ross, D. Staelin, E.P. Windsor, F.T. Barath, P. Gudmansen, E. Langham and R.O. Ramseien, "A summary of results from the first Nimbus and SMMR observations," *Journal of Geophysics Research*, vol. 89, pp. 5335-5344, 1984.
- Goodberlet, M. A., C. T. Swift, and J. C. Wilkerson, "Remote sensing of ocean surface winds with special sensor microwave imager," *Journal of Geophysics Research*, vol. 94, no. C10 pp. 14,574-14,555, October 1989.
- Goodberlet, M.A. and C.T. Swift, "Improved retrievals from the DMSP wind speed algorithm under adverse weather conditions," *IEEE Transactions on Geoscience and Remote Sensing*, vol. 30, pp.1076-1077, September 1992.
- Hayes, S.P., L.J. Magnum, J. Picacut, and K. Takeuchi, " TOGA-TAO; A moored array for real time measurements in the tropical Pacific Ocean," *Bulletin of American Meteorological Society*, vol 72, pp. 339 - 347, 1991.
- Hollinger, J.P., "Passive microwave measurements of the sea surface," *IEEE Transactions on Geoscience and Remote Sensing*, vol. 91, pp. 165-169, 1971.
- Hollinger, J.P., R. Lo, G. Poe, R. Savage, and J. Pierce, *Special Sensor Microwave Imager User's Guide*, Naval Research Laboratory, Washington, D.C., September 1987.
- Hollinger, J.P., *DMSP Special Sensor Microwave Imager Calibration/Validation*, final report vol II, Naval Research Laboratory, Washington, D.C., May 1991.
- Krasnopolsky, V.M., L.C. Breaker, and W.H. Gemmill, "Development of a single All-Weather Neural Network algorithm for estimating ocean surface winds from the special sensor microwave imager," *Technical Note*, National Meteorological Center, Washington, D.C., June 1994.
- Lo, R.C., "A comprehensive description of the mission sensor microwave imager (SSM/I) environmental parameter extraction algorithm," *NRL Memo. Rep.*, 5199, 1983.
- Monaldo, F.M., "Expected differences between buoy and radar altimeter

estimates of wind speed and significant wave height and their implications on buoy-altimeter comparisons," *Journal Geophysics Research*, vol. 93, no. C3, pp. 2285-2302, March 1988.

Schluessel, P., and H. Luthardt, "Surface wind speeds over the North Sea from special sensor microwave imager observations," *Journal Geophysics Research*, vol 96, no. C3, pp. 4845-4853, March 1991.

Smith, S.D., "Coefficients for sea surface wind speeds, heat flux, and wind profiles as a function of wind speed and temperature," *Journal of Geophysics Research*, vol 93, pp. 15467 - 15472, 1988.

Stogryn, A., "Radiometric emission from a rough sea surface," *Aerojet General Corporation Report*, no. 3000 R-1, 1972.

Stogryn, A.P., C.T. Butler, and T.J. Bartolac. "Ocean surface wind retrievals from special sensor microwave imager data with neural networks," *Journal Geophysics Research*, vol. 90, no. C1, pp. 981-984, January 1994.

Swift, C.T., "Special Joint Issue on Radio Oceanography," *IEEE Journal of Oceanic Engineering*, vol OE-2, no. 1, pp. 1-4, January 1977.

Swift, C.T., "Passive microwave remote sensing of ocean surface wind speeds in surface waves and fluxes," edited by G.L. Geernaert and W.L. Plant, Kluwer Academic Publishers, Dordrecht, 1990.

Ulaby, F.T., R.T. Moore, and A.K. Flung, *Microwave Remote Sensing Active and Passive*, Vol. 3, Artech House, Norwood, Ma, 1986

Wentz, F.J., "Measurement of oceanic wind vector using satellite microwave radiometers," *IEEE Transactions on Geoscience and Remote Sensing*, vol. 30, no. 5, pp. 960-972, September 1992.

INITIAL DISTRIBUTION LIST

	No. Copies
1. Defense Technical Information Center Cameron Station Alexandria, Virginia 22304-6145	2
2. Library, Code 52 Naval Postgraduate School Monterey, California 93943-5101	2
3. Combat Systems Academic Group, Code 33 Naval Postgraduate School Monterey, CA 93943-5000	1
4. Department of Physics Attn: Professor R. C. Olsen, Code PH/OS Naval Postgraduate School Monterey, CA 93943-5000	3
5. FNMOC/Code 73 Attn: Dr. M. C. Colton 7 Grace Hopper Ave, Stop 1 Monterey, CA 93943	2
6. NRL, Code 7211 Attn: Gene Poe 4555 Overlook Ave Washington, D.C. 20375-5320	1
7. University of Massachusetts Attn: Mark Goodberlet Amherst, MA 01003	1
8. AFGWC, Code DOA Attn: Charles Holiday Offutt AFB, NE 68113	1

